Inner Shelf Dynamics Science and Experiment Plan

by Falk Feddersen[1], Jack Barth[2], Joe Calantoni[3], Chris Chickadel[4], John Colosi[5], Emanuele Di Lorenzo[6], Chris Edwards[7], Gordon Farquharson[4], Thomas Freismuth[5], Hans Graber[8], Kevin Haas[6], Mick Haller[2], Thomas H.C. Herbers[9], David Honegger[2], Tim Janssen[9], Nirnimesh Kumar[1], Luc Lenain[1], James Lerczak[2], Jennifer MacKinnon[1], Jamie MacMahan[5], James McWilliams[10], Ken Melville[1], Arthur Miller[1], Andrew Moore[7], Melissa Moulton[4], James Moum[2], Ad Reniers[11], Roland Romeiser[8], Julian Simeonov[3], Matthew Spydell[1], Eric Terrill[1], Jim Thomson[4], and Amy F. Waterhouse[1]

[1] *Scripps Institution of Oceanography*
[2] *Oregon State University*
[3] *Naval Research Laboratory, Stennis Space Center*
[4] *Applied Physics Laboratory, University of Washington*
[5] *Naval Postgraduate School*
[6] *Georgia Institute of Technology*
[7] *University of California, Santa Cruz*
[8] *Rosenstiel School of Marine and Atmospheric Science, University of Miami*
[9] *Northwest Research Associates*
[10] *University of California, Los Angeles*
[11] *Delft University of Technology*

Technical Report
APL-UW 1602
October 2016

Applied Physics Laboratory University of Washington
1013 NE 40th Street Seattle, Washington 98105-6698

Grant numbers: Calantoni, N0001416WX00044; Colosi, N0001415WX00691; Di Lorenzo, N000141410556; Farquharson and Chickadel, N000141512389; Feddersen, N00014512631; Graber and Romeiser, N000141612631; Haller, N000141512020; Janssen, N000141612856; Lerczak and Barth, N000141512617; MacKinnon and Waterhouse, N000141512633; MacMahan, N0001415WX00574; McWilliams, N000141512645; Melville, N000141512529; Miller, N000141410553; Moum, N000141512466; Terrill, N000141512614; Thomson, N000141512630

CONTENTS

1. Introduction

The deep ocean, continental shelf, and surf zone are defined by their unique physical processes and dynamics. The nearshore region from about 50 m water depth to the outer edge of the surf zone (SZ) is known as the inner shelf. This region is characterized by overlapping and interacting surface and bottom boundary layers. At the offshore side of the inner shelf, instabilities from wind-driven currents and fronts create cross-shelf meanders and eddies. In addition, energetic nonlinear internal waves (NLIWs) are ubiquitous on the inner shelf. The surf transition region (STR) is the most shoreward 1-km-wide region (depth < 15 m) of the inner shelf region and SZ.

The inner shelf is an important gateway between the SZ and the continental shelf for the transport of heat, sediment, entrained gases, nutrients, pollutants, and biota (Figure 1). Here waves, circulation, and temperature vary over a wide range of spatial and temporal scales, and are driven by an array of processes forced by variable coastal bathymetry. Processes on the inner shelf include turbulence generated at the boundary layer at <1 m (e.g., *Trowbridge and Elgar*, 2001; *Feddersen et al*., 2007), 50–100 m rip currents on time scales of minutes (e.g., *Marmorino et al*., 2013, Figure 1), shoaling and breaking NLIWs on time scales of one hour (e.g., *Shroyer et al*., 2011; *Walter et al*., 2012; *Sinnett and Feddersen*, 2014; *Zhang et al*., 2015), semidiurnal internal tides (e.g., *Winant*, 1974; *Lerczak et al*., 2003), wind-driven currents, fronts and eddies, subtidal rotation-influenced processes (e.g., *Lentz et al*., 1999, 2008), as well as seasonal variability (*Kohut et al*., 2004). Complex bathymetry, such as canyons and headlands, enhance the spatial variability of surface gravity waves, internal waves, wind forcing, and circulation in the inner shelf region (e.g., *Long and Özkan-Haller*, 2005; *Apotsos et al*., 2008; *Smit et al*., 2015) that drive exchanges onto the deeper shelf. Past studies have focused on either SZ (e.g., *Elgar et al*., 1997; *Feddersen et al*., 1998; *Herbers et al.,* 1999) or shelf (e.g., *Fewings et al*., 2008) processes, usually at sites with relatively uniform coastlines. Observations, however, of processes encompassing both the inner shelf and SZ are sparse, particularly near complex bathymetry.

Understanding the links between the inner shelf and surf zone are particularly important for U.S. Navy activities including watercraft and naval special warfare operations, mine hunting, beach landings, search and rescue, and shallow water acoustics. The U.S. Navy ocean forecasting system transitions from a global ocean 1/25° HYCOM model to a Delft3D in the nearshore region, including the SZ. To forecast ocean dynamics and stratification seamlessly from the deep ocean to the shoreline, there is a critical need to improve understanding and modeling capability of inner shelf processes and their spatial and temporal variability.

To understand and predict the exchange of water properties (heat, gases, sediment, pollutants, biota) across the inner shelf over a range of temporal and spatial scales, the Office of Naval Research Inner Shelf Dynamics Departmental Research Initiative (Inner Shelf DRI) is coordinating field observations (in situ and remote sensing) coupled to numerical modeling efforts on a 50-km section of coast off Vandenberg Air Force Base, California, located in the vicinity of Point Sal. The overall goal is to develop and improve the predictive capability of a range of numerical models to simulate the 3D circulation, density, and surface wave field across the inner shelf associated with a broad array of physical processes and complex bathymetry.

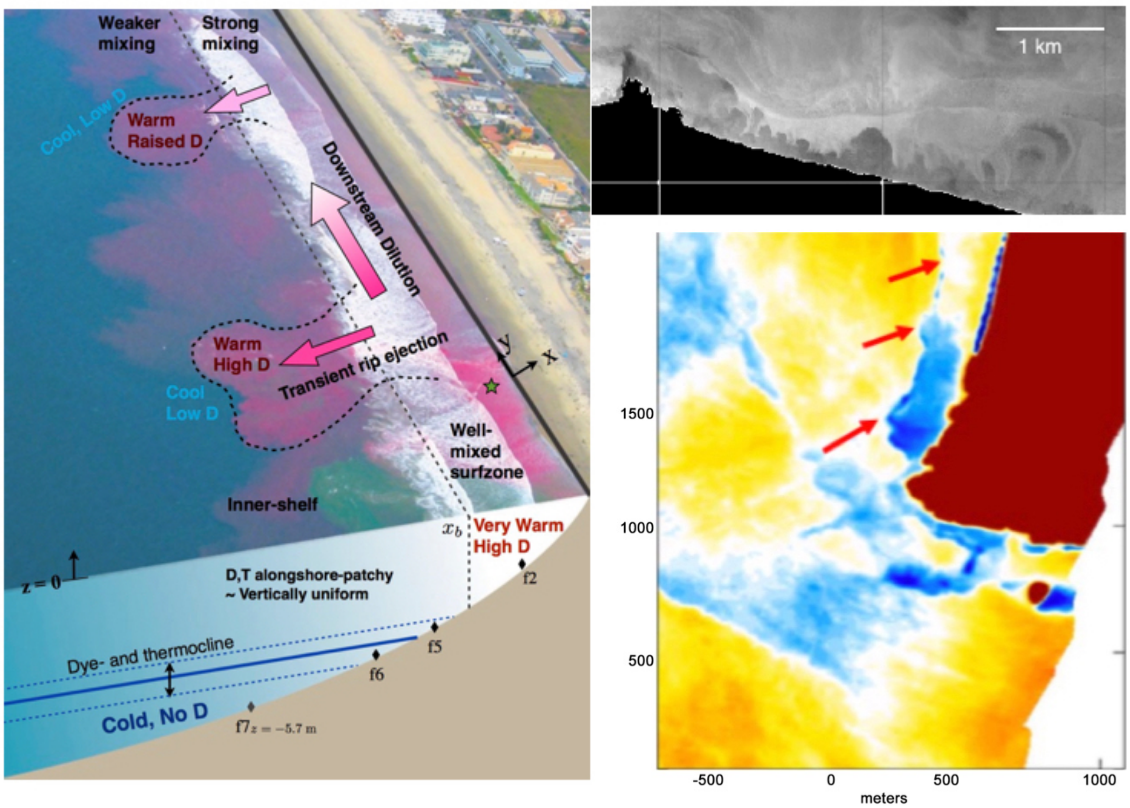

Figure 1. Components of the Inner Shelf DRI. (left) A warm surf zone (SZ) and colder inner shelf. Transient rip currents eject warm sediment-rich water onto the inner shelf as internal waves raise and lower the thermocline, at times pumping cold water to the shoreline. The inner shelf has both strong surface and bottom boundary layers and turbulence generated by internal waves. (right top) Thermal imagery of transient and bathymetrically controlled rip currents near a headland that eject cool SZ water up to 500 m onto the inner shelf at alongshore length scales of 50–500 m (*Chickadel*, DRI 2015 pilot experiment) and intersect with internal waves propagating into the STR. (right bottom) Long-wave infrared imagery of the Point Sal region spanning 2 km x 2 km shows the spatial range of eddies and internal wave processes. Red arrows show a temperature front (*Melville and Lenain,* DRI 2015 pilot experiment).

2. Background: Inner Shelf Processes

2.1. Stokes Drift

The exchange between the SZ and inner shelf flows is variable over depth, and the vertical flow structure is important to understand transport processes. For a uniform coast without rip currents or eddies, a difference in the mean Lagrangian flow due to surface waves (Stokes drift) and the Eulerian return flow (undertow) results in a net cross-shore exchange (Figure 2). Within the SZ, the onshore (Lagrangian) Stokes transport is generally not in local balance with the Eulerian return flow (undertow), again leading to cross-shore exchange (e.g., *Reniers et al*., 2004; Figure 2).

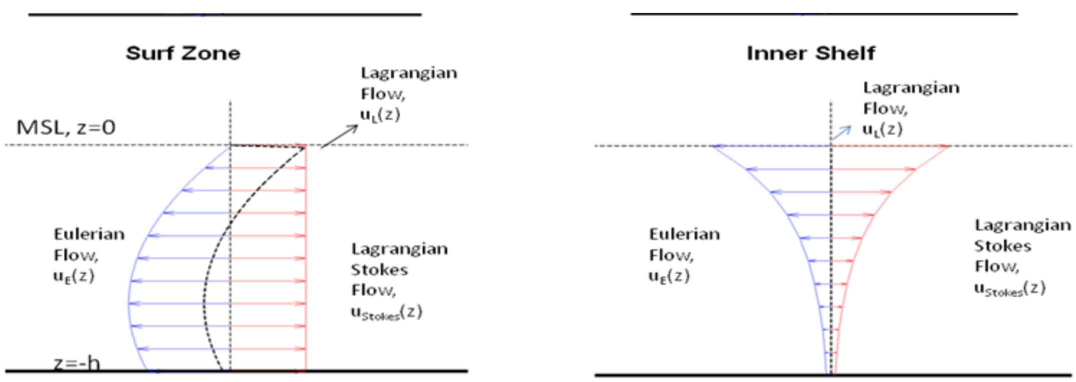

Figure 2. Wave and background flow description for a beach that is homogeneous alongshore in the Lagrangian frame of reference for (left) a typical SZ and (right) for a shallow inner shelf with weak vertical mixing (e.g., *Lentz et al*., 2008). Mean sea level is the horizontal dashed line. Seabed is the horizontal solid line. Vertically oriented dashed lines in both panels represent the total Lagrangian (Stokes and Eulerian) flow. Figure prepared by J. MacMahan.

On the inner shelf, the dynamics are more complicated than an ideal uniform coast and not as well understood. Long-term inner shelf observations show that the Eulerian return average flow can be in balance with the onshore Stokes drift, resulting in no net exchange (*Hasselmann*, 1970; *Xu and Bowen*, 1994; *Lentz et al*., 2008; *Kumar et al*., 2012). This balance, however, depends on local wind stress, vertical mixing, surface wave dynamics, stratification, and coastal bathymetry. Theoretically, it seems questionable that in the presence of wind such a steady balance can be maintained (e.g., *Polton et al*., 2005; *Aiki and Greatbatch*, 2012). For example, the presence of strong wind stresses over the inner shelf can result in either offshore or onshore transport, and the controlling mechanisms are not clear (*Fewings et al*., 2008; *Fujimura et al*., 2013).

Despite the advances in the theoretical understanding of wave-driven flow dynamics (*Xu and Bowen*, 1994; *Mellor*, 2003; *McWilliams et al*,. 2004; *Ardhuin et al*., 2008; *Aiki and Greatbatch*, 2012, 2013) and increasing awareness of the implications and importance of Stokes drift for general circulation models (e.g., *McWilliams and Restrepo*, 1999) and cross-shelf mass transport (e.g., *Lentz et al*., 2008; *Fewings et al*., 2008; *Lentz and Fewings*, 2012), most theoretical models and observations consider fairly idealized conditions and/or uniform coastlines. In more complicated regions, such as the coastline around Point Sal, California, the effects of an inhomogeneous and nonstationary surface wave field (resulting in spatial and temporal variability of the mean Stokes drift), infragravity Stokes drift fluctuations (*Herbers and Janssen*, 2016), and interactions with complex bathymetry have not been studied.

2.2. Rip Currents

Rip currents (both transient and bathymetrically controlled) eject water onto the inner shelf (Figure 1). For a coast with alongshore uniform bathymetry, rip currents form due to SZ input of vorticity due to breaking of a directionally spread wave field at wave group and individual wave time scales (e.g., *Reniers et al*., 2004; *Johnson and Pattiaratchi*, 2006; *Long and Özkan-Haller*, 2009; *Feddersen*, 2014). This vorticity evolves and leads to eddy ejection events from the SZ onto the inner shelf, or transient rip currents and exchange (*Suanda and Feddersen*, 2015). The frequency and length scales of rip ejection events have not been characterized.

Dye tracer (*Clark et al*., 2010) and SZ surface drifter (*Spydell et al*., 2009; *Reniers et al*., 2009; *MacMahan et al*., 2010; *Brown et al*., 2015) experiments show that dye and drifters are retained within twice the SZ width (≈ 100−200 m from the shoreline) over the span of a few hours. Observations of surface roughness generated by rip currents indicate that even moderate near-surface rip currents can extend multiple SZ widths offshore (*Haller et al*., 2014). Surf zone eddies ejected to the inner shelf can also generate an exchange barrier (*Reniers et al*., 2010). Variable alongshore inner shelf bathymetry at a range of spatial scales from rip channels to headlands can induce inhomogeneity in the mean flows and wave conditions, and promote exchange. For example, on coasts with well-defined rip channels, the SZ is estimated to be flushed (and replenished) on the time scale of hours, yet most of this flushed water is returned to the SZ (e.g., *MacMahan et al*., 2010). Exchange driven by rip currents near complex bathymetry (headlands), however, has not been studied.

Understanding of exchange across the inner shelf at longer time scales is also limited. For example, the processes whereby vertically well-mixed (i.e., unstratified) SZ water is ejected onto the stratified inner shelf have not been characterized. Fluid motion scales outside the SZ are hypothesized to be larger than within the SZ because they are associated with sub-mesoscale eddies, large-scale ambient flows (including upwelling, downwelling, and relaxation events), and (breaking) internal waves, among other processes. Hence the persistence, cross-shore extent, and orientation of mean and turbulent flows in the SZ will depend on inner shelf current dynamics. Lastly, complex bathymetry, such as the region near Point Sal, will induce exchange. Other exchange mechanisms are likely that have not yet been observed.

A simulation of an idealized stratified SZ and inner shelf with alongshore uniform bathymetry using the coupled COAWST and funwaveC models demonstrates the complexity of inner shelf dynamics (Figure 3). Directionally spread waves generate SZ eddies leading to transient rip currents that eject onto the inner shelf. These inner shelf eddies have vertical velocity drawing up colder water from below, strongly influencing the inner shelf temperature structure. After 18 hr, the inner shelf cools and the stratification decreases much more rapidly than without transient rip currents (*Kumar and Feddersen*, 2016). The temperature structure in the simulations is in agreement with features observed in aerial infrared (IR) images of the STR (Figure 1, top right; *Chickadel and Farquharson*, DRI 2015 pilot experiment). Simulation results of STR evolution have not yet been observed in the field. Note that the STR simulations did not consider internal wave processes and spatially variable bathymetry.

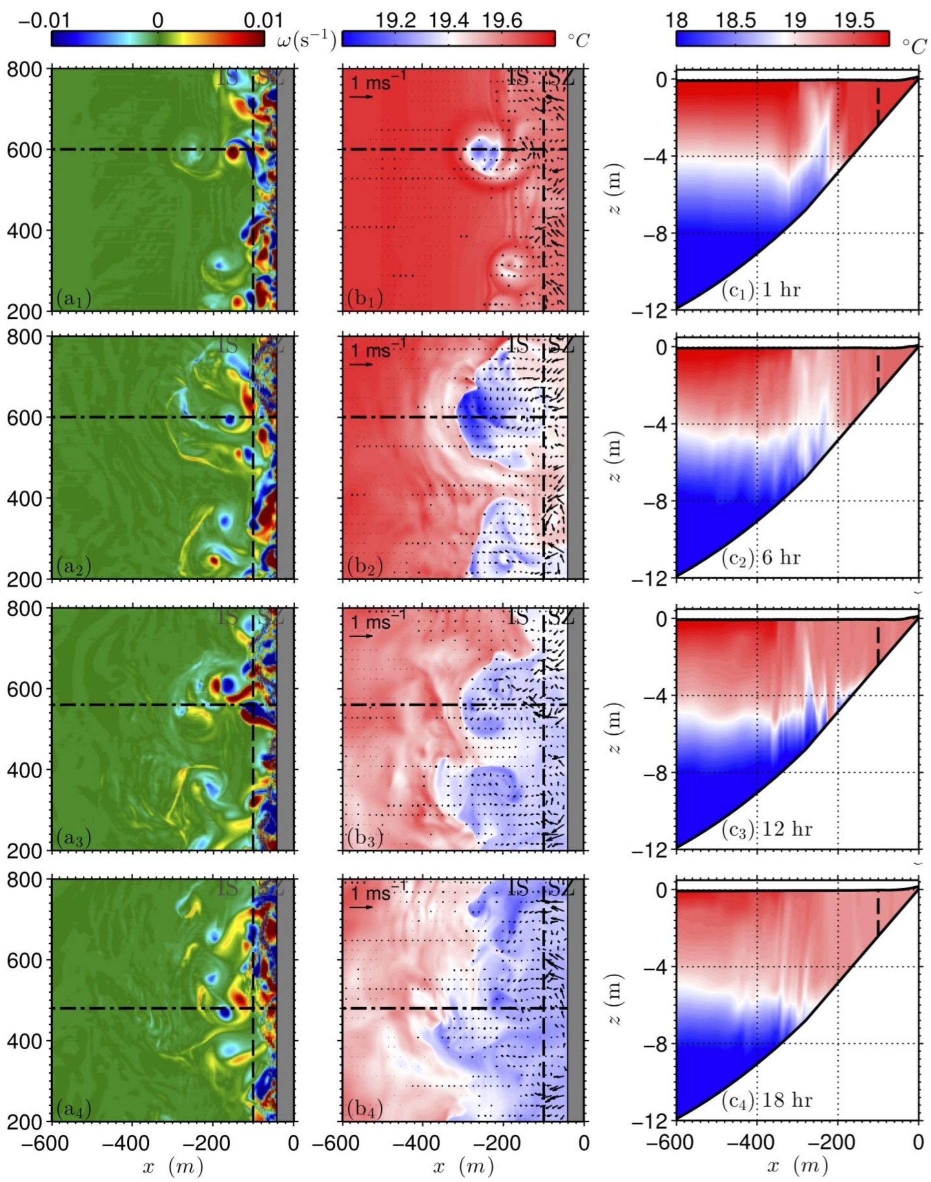

Figure 3. Simulated temperature (a_1–a_4) and vertical vorticity (b_1–b_4) at z = −1 m versus cross-shore x and alongshore y coordinates, and temperature (c_1–c_4) versus cross-shore x and vertical z coordinates at the dash-dot line at times 1 (a_1–c_1), 6 (a_2–c_2), 12 (a_3–c_3), and 18 (a_4–c_4) hr. Note, there is no surface heating (sunlight) in this simulation. From *Kumar and Feddersen* (2016).

2.3. Surface Waves

Surface waves force many inner shelf processes that drive cross-shelf circulation and exchange. Refraction and sheltering over complex coastal bathymetry can cause spatial inhomogeneity in the wave field (e.g., *Janssen et al*., 2008; *Smit and Janssen*, 2013); this can contribute directly to two-dimensional circulation and transport across the inner shelf (e.g., *Apotsos et al*., 2008; *Long and Özkan-Haller*, 2005; *Hansen et al*., 2014; *Smit et al*., 2015). The spatial inhomogeneity of the surface wave field causes variability in Stokes drift, which affects the local balance between Lagrangian wave-driven flows and Eulerian return flows. In random waves, the mean Lagrangian flow is modulated on wave group scales (e.g., *Srokosz and Longuet-Higgins*, 1986; *Smith*, 2006; *Herbers and Janssen*, 2016), the frequencies of which are much lower than the dominant wind waves and swell, but generally much higher than the vertical component of the Earth rotation vector, so Coriolis effects are small. These infragravity Stokes drift fluctuations are important for inner shelf tracer diffusion (e.g., *Herterich and Hasselmann*, 1982; *Sanderson and Okubo*, 1988; *Bühler and Holmes-Cerfon*, 2009), and may contribute to cross-shelf exchange.

As surface waves propagate across the inner shelf into shallow water, energy is transferred to (Eulerian) infragravity waves, whose modulations are amplified near the coast (e.g., *Herbers et al*., 1995; *Janssen et al*., 2003), and radiated back offshore through the STR. The outgoing radiation of infragravity waves depends on wave generation, reflection, trapping, and dissipation in the nearshore (*Herbers et al*., 1995). These processes are not well understood, particularly the rarely observed reflection and trapping of infragravity waves along a variable coastline in the presence of headlands.

2.4. Turbulence

The inner shelf is a region where the air–sea and the seafloor boundary layers either overlap or are separated by a pycnocline. Here, turbulence can be generated by bottom friction, internal wave breaking, surface wave breaking (whitecapping), and ejection of turbulence from the surf zone. Water column turbulence alters velocity and density profiles, in turn influencing exchange and mixing of water masses through the inner shelf region. For example, inner shelf cross-shelf exchange is critically dependent on the structure of the turbulent Reynolds stresses (*Lentz and Fewings*, 2012). Currently, direct measurements of inner shelf turbulence are rare, and the temporal and spatial variability of turbulence in this region is not well understood.

Microstructure profiles obtained during the Coastal Mixing and Optics DRI took place over two seasons with two different background states (*MacKinnon and Gregg*, 2003). During springtime, the water was initially weakly stratified, with surface and boundary layers together comprising most of the water column. Turbulence, as measured by a turbulence microstructure profiler, was strong within the upper and lower boundary layers and weak in between. A series of passing storms produced strong shear from inertial motions in the stratified water in between the upper and lower boundary layers. The resultant downward turbulent heat fluxes allowed the deeper water to warm and stratify, which in turn changed the nature of both the internal waves and the turbulence they produced. Proper predictive ability for this type of seasonal evolution requires improved dynamical understanding of the turbulent fluxes. During the summer experiment, the water was much more stratified and surface wind stress was weak. Turbulence in the stratified water between boundary layers was largely controlled by the internal tide propagating shoreward from the shelf break, especially when strongly nonlinear solitons were present. Such solitons typically have periods of only minutes, small horizontal scales, and are highly turbulent (*Moum et al*., 2003).

2.5. Internal Waves

Stratification and circulation on the inner shelf are strongly influenced by the arrival of NLIWs propagating from offshore with periods ranging from minutes to semi-diurnal (*Winant*, 1974; *Leichter et al*., 1998; *MacKinnon and Gregg*, 2003; *Moum et al*., 2003; *Walter et al*., 2012; *Scotti and Pineda*, 2004; *Suanda et al*., 2014). These internal motions are ubiquitous in the coastal ocean and are often formed by the barotropic tides forcing stratified fluid across the continental slope bathymetry or from remotely generated internal tides propagating toward the coast (*Nash et al*., 2012). As these NLIWs propagate across the complex bathymetry of the inner shelf, they refract, shoal, steepen, and break, altering the nearshore stratification, currents, and mixing. Questions remain about this transformation process across the inner shelf and how these internal motions influence cross-shore exchange from the SZ to the mid-shelf.

Analysis of in situ observations, numerical simulations, and laboratory studies have shown that these subsurface bore-like features have large pycnocline displacement, contribute to vertical and horizontal mixing, cause changes in stratification and circulation patterns, and transport nutrients, pollutants, biota, and sediments across the outer to inner shelf (*Melville and Helfrich*, 1987; *Helfrich*, 1992; *Butman et al*., 2006; *Scotti et al*., 2008; *Lucas et al*., 2011; *Alford et al*., 2012; *Walter et al*,. 2012, 2014a, b; *Woodson et al*., 2011; *Woodson*, 2013; *Zhang et al*., 2015). Stratification changes induced by NLIWs alter the waveguide and wave propagation. NLIW breaking may drive mean (wave-averaged) cross-shore density gradients, momentum flux divergences, and currents (*Hogg*, 1971), analogous to breaking surface waves in the SZ. Internal waves contribute to the nearshore heat budget by transporting cold sub-thermocline water (*Sinnett and Feddersen*, 2014) or super-thermocline water (*MacMahan*, DRI 2015 pilot experiment) into the SZ. The complexity of the inner shelf internal wave field increases near complex bathymetry such as that at Point Sal.

In situ observations of the internal wave field in the inner shelf are sparse and do not resolve internal wave interactions with varying bathymetry and currents. Satellite-based synthetic aperture radars (SAR) provide snapshots of surface roughening (e.g., *Jackson and Apel*, 2004) and surface velocities (e.g., *Romeiser and Graber*, 2015) associated with internal wave surface convergences. Fixed and aircraft-based radar (e.g., *Plant et al*., 2010), lidar, and thermal infrared (TIR) cameras (e.g., *Marmorino et al*., 2004) can map internal wave signatures repeatedly as a wave packet propagates across the shelf (Figure 1). Radar remote sensing can be effective at sampling the STR. Marine radars are used commonly to image surface waves, coastal fronts, and internal waves (e.g., *Chang et al*., 2008). These systems can image surface gravity waves in circular image footprints of radius 2–4 km when operating at their highest resolution and depending on sea state. Furthermore, ship-based X-band radars can observe the evolution of internal wave packets as they shoal and approach the shore (*Ramos et al*., 2009; *Lund et al*., 2013). Using shore-based radars, long dwell and image filtering techniques enable observations of internal wave propagation across the inner shelf over larger distances (up to 10 km). New methods must also be developed to combine airborne and fixed radar, SAR, lidar, and IR observations with in situ observations.

2.6. Wind Forcing

On the inner shelf, wind-driven surface and bottom boundary layers interact, fundamentally altering the balance of forces that control stratification and currents (Figure 4; *Austin and Lentz*, 2002). Wind-driven, cross-shelf currents on the inner shelf decrease because of the coastal boundary. Along-shelf currents can span the entire water column reaching the bottom to re-suspend sediment. The cross-shelf and along-shelf currents driven by along-shelf winds acting on a stratified coastal ocean are fundamentally different whether winds are favorable for upwelling or downwelling. For example, during downwelling the cross-shelf circulation is suppressed inshore of the downwelling front leading to a trapping of buoyant material at the front location and its subsequent transport alongshore over long (100–1000 km) distances (*Austin and Barth*, 2002).

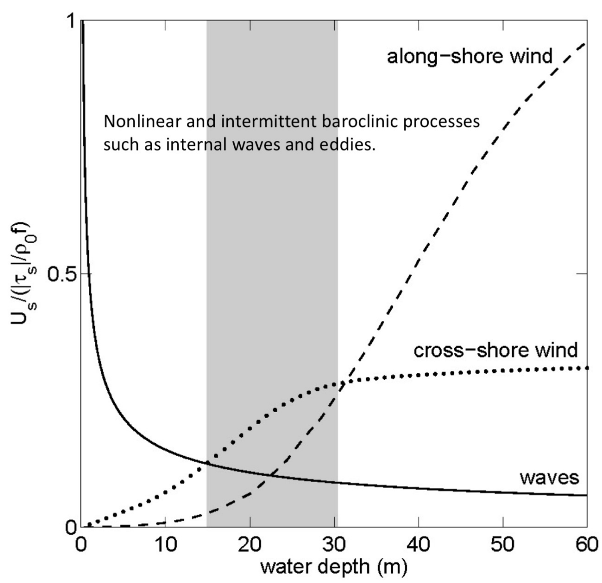

Figure 4. Ratio of wave to wind forcing on the inner shelf of the theoretical cross-shore surface layer transport normalized by the deep-water Ekman transport. Waves are greatest for <15 m depth, whereas wind forcing is greatest for >30 m depth. In intermediate depths (gray shaded region). Baroclinic processes such as nonlinear internal waves drive variability in currents, stratification, and mixing within the inner shelf. Adapted from *Fewings et al*. (2008).

It is well known that vertically and horizontally sheared currents associated with upwelling and downwelling fronts in the mid-shelf can become unstable to create along-front meanders and, eventually, eddies that contribute to cross-front exchange (*Barth*, 1989a, b; 1994). Observations of eddies reveal that they are an important source of lateral exchange for surface waters over the inner shelf (*Kirincich*, 2016). Recent numerical simulations show the creation of meanders and eddies on a wind-driven coastal upwelling front off Oregon (*Durski and Allen*, 2005). Meanders have wavelengths of 5–10 km, and resulting eddies are 2.5–5 km in diameter. Much less is known about these unstable wind-driven jets and fronts when they are close to the inner shelf, including how they contribute to exchange between the mid- and inner shelf.

3. Science Questions and Goals

The overall goal is to improve understanding of inner shelf hydrodynamics, and develop and improve the predictive capability for a range of numerical models to simulate accurately the 3D flow and temperature evolution across the inner shelf, particularly in regions of complex bathymetry. To achieve this goal, we propose a multi-investigator field experiment that combines intensive in situ and remote sensing observations of flow and temperature evolution along a highly variable, 50-km coastline section at Point Sal, CA (Figure 5). The specific questions and goals for the experimental study include:

- To what extent is the Eulerian cross-shore flow in the inner shelf in balance with the onshore directed, wave-driven Stokes drift as suggested by *Lentz et al*. (2008), and over what time scales? How important are Stokes–Coriolis forces to the mean circulation dynamics on the inner shelf, particularly in regions of complex bathymetry?
- What are the alongshore scales of transient and stationary rip currents and how do they depend upon the distance from the SZ boundary? How often do ejection events occur and what are their fluxes? How do rip currents interact with flows driven by headlands?
- How do the bathymetry, stratification, and coastal flow features (e.g., headland eddies, relaxation) impact internal wave evolution? How does this change over time?
- What are the principal dynamic and topographic causes of alongshore and across-shore variability of NLIWs on the inner shelf? What are the processes modulating NLIW activity?
- What governs the location of NLIW dissipation and associated mixing (isobath and depth/isopycnal)? How does this evolve in response to lower frequency variability? How does this affect the background stratification?
- What are the net onshore and alongshore fluxes of mass, heat, salt, and momentum driven by NLIWs?
- What relative roles do wave-driven Stokes drift, transient and stationary rip currents, internal waves, wind forcing, buoyancy, and rotation have in driving cross-shelf exchange in uniform and complex coastal bathymetry?
- What relative roles do turbulence generated at the seafloor boundary, wave breaking at the surface boundary, and breaking internal waves have in stratification and mixing in the inner shelf? How often and why do surface and bottom boundary layers overlap?
- How is the reflection and trapping of infragravity waves affected by along-coast variability and complex bathymetry? What are the implications for offshore radiation of infragravity wave motion?
- What roles do diurnal sea breezes have in driving cross-shelf exchange and inducing lateral gradients in surface wind stress?

We propose to address these questions through a multi-investigator, collaborative field experiment that will capture the range of processes and scales on the inner shelf in a region of complex bathymetry. Specifically, the experiment will have the following components:

- Collect in situ and remote sensing wave observations that capture the regional surface wave variability (both cross- and alongshore). This will quantify regional variability in wave forcing to dynamical balances. Synoptic wave measurements will be available to the Inner Shelf DRI research groups. Wave observations will support validation of remote sensing observations and advance models for random, nonlinear surface wave propagation on the continental shelf.
- Deploy an integrated array of in situ ADCPs, thermistor chains, conductivity sensors, GusT probes, and pressure sensors to measure waves, tides, water temperature, salinity, and ocean currents with which to address the above research hypotheses including measuring inner shelf cross-shelf exchange. These in situ observations will also validate and be integrated with remote sensing observations.
- Collect an array of short- and long-dwell remote sensing observations and include satellite, marine radar, IR, lidar, hyperspectral imagery, and SAR that cover a range of temporal and spatial scales across the inner shelf.
- Deploy SZ and shelf drifters across the STR and track the Lagrangian flow pathways.
- Conduct cross- and alongshore surveys of the inner shelf with shipboard instruments to measure variability in currents, temperature, salinity, and turbulence due to shoaling NLIWs, wind driven processes, and eddies.

This experiment will establish the dominant length and time scales of inner shelf processes, and determine the cross-shore extent and temporal variability of cross-shelf exchange in the presence of complex bathymetry. The observations from this new field experiment will be used to test and improve model predictions with a focus on the 3D evolution of the flow and temperature structure at a broad range of scales — from surface gravity and internal waves, to Stokes drift and rip currents. This effort will explain the transport of water masses between the SZ and inner shelf, particularly near complex bathymetry, and result in improved modeling capability validated with detailed field measurements. For example, analysis of the combined data set will be used to identify episodic flow events, such as rip currents and internal waves, and quantify their frequency of occurrence and their importance to exchange processes. These diverse observations will aid development of methods to map evolving internal wave packets on the inner shelf. Inner shelf internal wave evolution observations will be used to study the feedback between internal waves, stratification, circulation patterns, and cross-shelf exchange. In situ turbulence observations will determine the most relevant processes affecting mixing and the exchange of water masses across the inner shelf.

4. Strategy

4.1. Experiment Site

The field experiments will be conducted around Point Sal, CA, which is located between two relatively straight shorelines referred to as Pismo Beach to the north and Vanderberg Beach to the south (Figure 5). Point Sal, a 7.5 km-wide headland, is located between Point Buchon (28-km headland) to the north and Point Purisma (7-km headland) to the south. Point Buchon and its mountain range create a shadow region on the south side inducing an alongshore gradient in wave energy and wind stress for Pismo Beach. This alongshore gradient in wave energy results in alongshore variation in SZ morphology. There is an absence of SZ morphology on the north end of Pismo Beach. Moving toward the south end of Pismo Beach, rip channeled bathymetry becomes increasingly the dominant morphology. There is a small pocket at Point Sal owing to the Point Sal rocky headland and a small rocky headland to the north, referred to as Mussel Point. The west-facing shorelines are predominantly sandy beaches, whereas the south-facing shorelines are rocky. Directly offshore of Point Sal there is a subaqueous rocky quasi-circular outcrop. There are additional subaqueous outcrops offshore of Vandenberg Beach and Point Purisma.

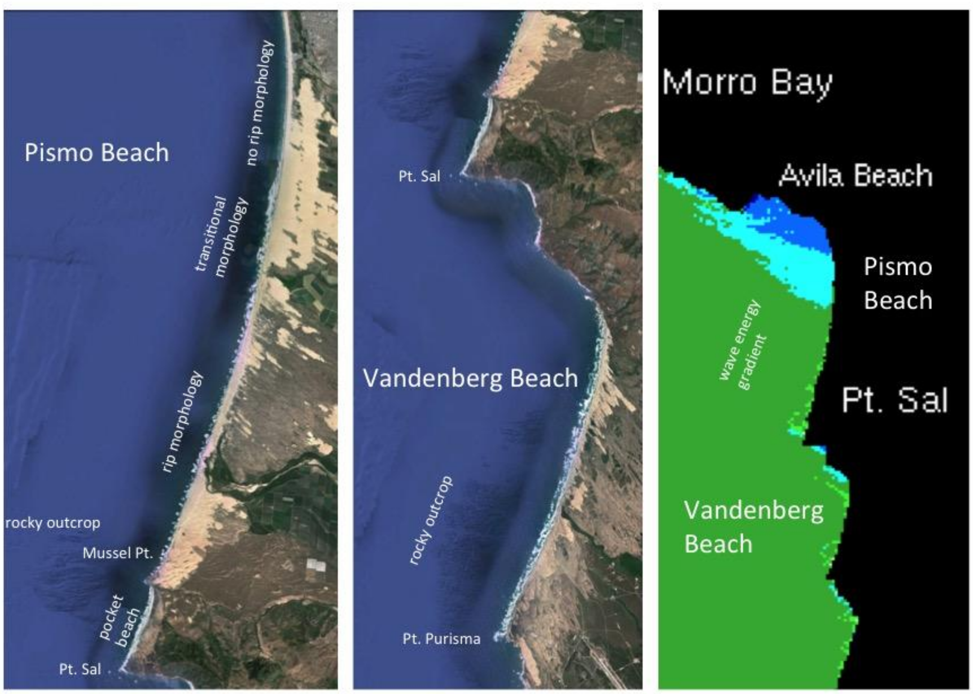

Figure 5. Maps of (left) coastal region north of Point Sal showing morphology classifications (middle) and region south of Point Sal to Point Purisma, and (right) Coastal Data Information Program real time wave height image showing incident wave height variability particularly due to sheltering from Point Buchon and Point Sal.

4.2. In Situ Observations

4.2.1. Temperature, Salinity, and Velocity Moorings (MacMahan, Feddersen, Reniers, Lerczak, Barth, MacKinnon, Waterhouse, Colosi)

In situ temperature and conductivity moorings and ADCPs will be deployed in the experiment region. Within the STR, these moorings will be split into eight Mini-STR arrays, 11 co-deployed ADCP and T-chain moorings, and 13 stand-alone thermistor chains. Mini-STR temperature arrays including ADCPs will be deployed in ~8 m water depth (outside of the SZ) at eight different locations along the 30-km stretch of coastline, obtaining measurements associated with different SZ morphologic scales and topographic features (e.g., rocky headlands, points, or subaqueous outcrops; Figure 6, dark green circles and stars). The mini-STR arrays will estimate the directional temperature patterns of subtidal motions, internal waves, and SZ exchange. The mini-STR arrays are composed of five elements, where each element consists of a vertical array of temperature sensors (Figure 7). The vertical thermistor array will measure the stratification structure, internal wave characteristics, and vertical mixing. The cross-shore array will extend across one SZ width representing the STR. In each array, one ADCP will be collocated with a temperature string. Cross-shore or alongshore fluxes will be estimated with the arrays.

In addition, 11 co-deployed ADCPs and T-chains with 6–8 thermistors together with 13 T-chains moorings (without ADCPs) will be deployed in the 8–18 m depth region from just south of Point Sal to just north of Mussel Point, the region of greatest coastline and bathymetric complexity. These locations will constrain the along-coast fluxes of mass and temperature and also resolve internal wave propagation directly incident onto Point Sal (Figure 6, cyan circles and stars).

Farther offshore, moorings and bottom landers to measure NLIWs and wind-driven processes will be deployed at 50–120 m depth (Figure 6, light green stars). A single mooring–bottom lander pair will be deployed on the 100-m isobath (thermistors, CT sensors, and ADCP) to measure internal tides and NLIWs incident on the study site. Four thermistor/CT moorings (two with bottom landers and ADCPs) will be deployed along the 50-m isobath to measure internal wave and wind driven variability across the study site. Two arrays will target processes at the straight beach near the Guadalupe River (13 thermistor/CT moorings and 11 bottom-mounted ADCPs) and offshore of Mussel Point (six thermistor/CT moorings and six bottom-mounted ADCPs). These arrays are designed to measure the evolution of the nonlinear internal wave field in water depths of 35–100 m to determine the influence of bathymetry on NLIW propagation (shoaling, refraction, focusing, and breaking), and to serve as a control volume array to quantify NLIW momentum fluxes and flux divergences, and net fluxes of mass, salt, and heat due to NLIWs.

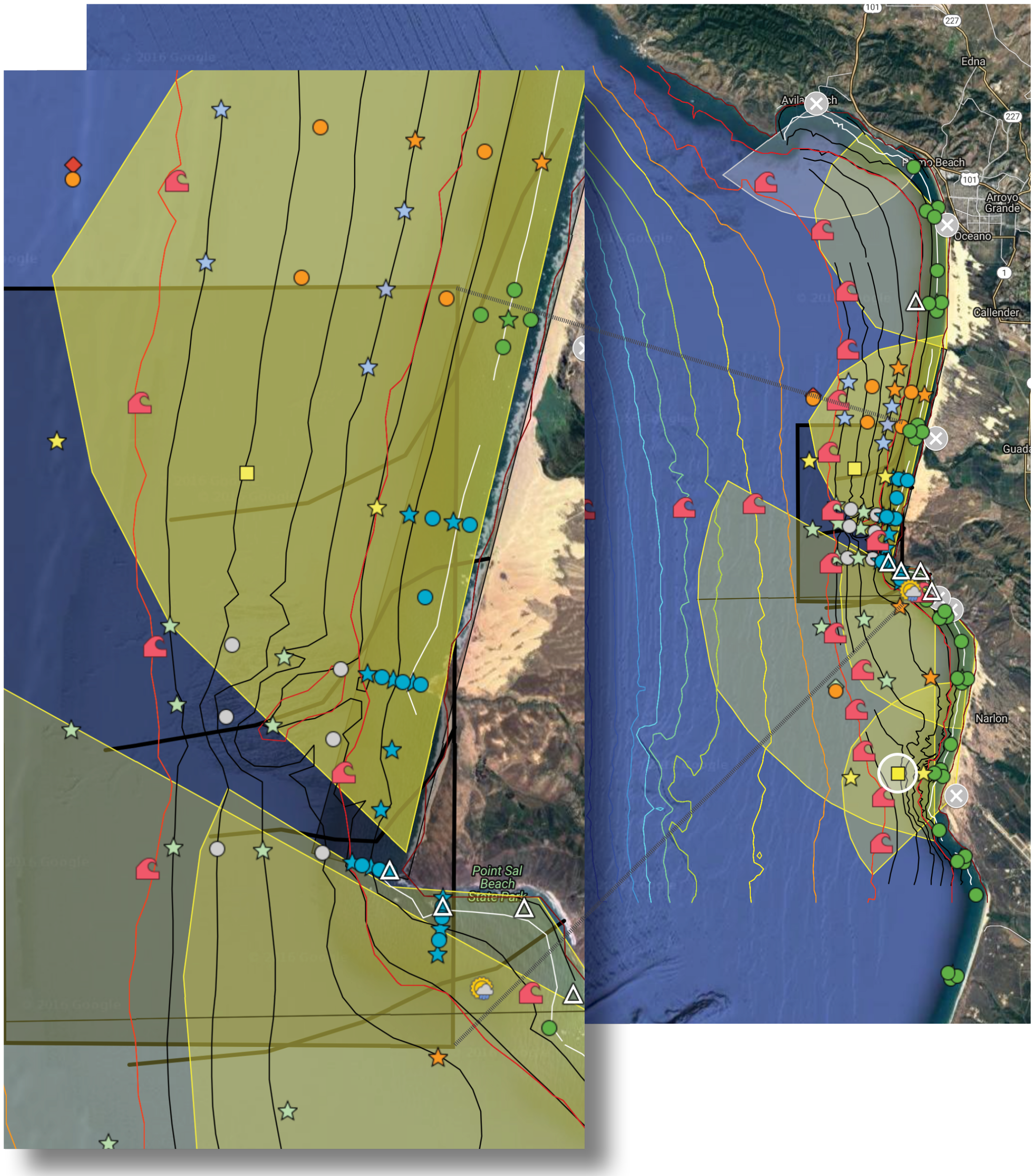

Figure 6. Inner Shelf DRI experiment site: (base, right) large-scale view and (inset, left) Point Sal focus region. Instrumented locations include wave observations (red waves), STR ADCP and T-chains (cyan stars), STR T-chains (cyan circles), STR five-element T-chain array with ADCP (dark green stars and circles), NLIW ADCP and CTD moorings (orange stars and circles, also light green stars), turbulence quadpods (yellow stars and squares), bottom landers (white triangles), T-chains (gray circles), marine radar field of view (yellow shaded regions), and flight box for SAR and surface temperature (gray rectangle). Lagrangian drifters will be deployed within the inner domain. Link to Google Maps representation of the Inner Shelf DRI experiment site and observational assets:
https://www.google.com/maps/d/edit?mid=1_ENwUAes01WNkfek2djoEQJKzV8

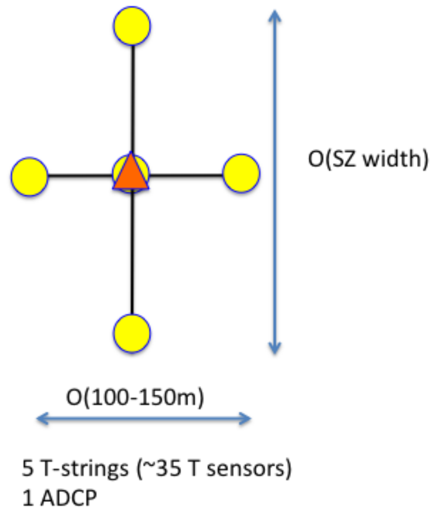

Figure 7. Schematic of the mini-STR array with five vertical thermistor strings (circles) spanning approximately 150 m cross- and alongshore, and an ADCP (triangle) in the Mini-STR array center.

4.2.2. Surface Wave Moorings (Janssen, Herbers, Terrill)

Moorings, each with a surface tracking buoy and a collocated pressure sensor, will be deployed at the experiment site (18 moorings are planned; Figure 6, red waves). Combining a Lagrangian surface-following instrument and an Eulerian pressure sensor aims to resolve the primary wave field and infragravity components, and identify Lagrangian effects in the infragravity motion, which are generally far more energetic than the Eulerian components at intermediate water depth (*Herbers and Janssen*, 2016). The instruments will be deployed in two alongshore arrays, on the 20 m and 50 m depth contours, and include one cross-shore transect to capture the cross-shelf transformation. The alongshore arrays will extend along the entire research area to measure the alongshore variability and provide complete boundary conditions for modeling studies. Instruments will be concentrated around areas of increased complexity (e.g., Mussel Point, and/or Purisima Point). The moorings are lightweight and mobile, and will be deployed from a UNOLS vessel, to be coordinated with other researchers. A GPS-based wave measuring buoy will be deployed in the footprint of the X-band radar (Figure 6), approximately 3 km offshore.

4.2.3. Near-bed Turbulence Quadpods (Calantoni, Simeonov)

A trio of bottom moorings will be deployed in a cross-shore transect to quantify the vertical structure of the turbulent eddy viscosity in the bottom boundary layer during the passage of upwelling/downwelling fronts across the inner shelf (Figure 6, yellow stars and square to the south). One quadpod will be located inside the STR in the field of view of a ground-based radar station, and a second quadpod will be located just outside the

STR. A third, smaller mooring containing an uplooking ADCP and vertical thermistor string will be located near the 50-m depth contour to complete the cross-shore transect.

A second identical transect (subject to instrumentation availability) will be deployed alongshore at least 10 km to the north (Figure 6, yellow stars and square to the north). Each of the four proposed quadpods will be instrumented with stacked, synchronized Acoustic Doppler Velocimeters (ADVs), HR-Aquadopps, CTDs, scanning sonars to quantify local seafloor roughness, and vertical thermistor chains to monitor the vertical structure of various parameters (waves, currents, temperature, conductivity, turbulence intensity) in the water column and in the bottom boundary layer.

4.2.4. High-resolution Seafloor Pressure Sensors (Moum, Nash)

Seafloor pressure sensors (6–10) will be deployed to detect evolving cross-shelf gradients and nonlinear internal waves. Several of these will be attached to experiment landers and several fully autonomous units will be deployed from a vessel (or helicopter) and recovered by an acoustic trigger release method.

4.2.5. GusT Probes (Moum, Nash)

GusT probes (80) specially designed for this experiment will be configured to mate with as many instrument platforms as possible. The basic sensor configuration includes a fast thermistor, identical to that deployed continuously on equatorial moorings since 2005 (*Moum and Nash*, 2009). Uniquely, it includes a new velocity sensor that measures mean flow speed at a point plus the fluctuating components that comprise the spectrum of turbulence. This differential pressure measurement of velocity includes common-mode compensation to reduce biases from absolute pressure, temperature, and accelerations (*Moum*, 2015).

4.2.6. Bottom Landers (Thomson, Moulton)

The mooring array will be supplemented with bottom landers (Figure 6, white triangles): one Acoustic Wave and Current Profiler (AWAC, 1 MHz) at 20 m water depth, two Aquadopps (2 MHz) at 10 m depth, and two ADVs (6 MHz) at 5 m depth. The goal is to measure waves and current profiles on an hourly duty cycle throughout the experiment. The locations are to be determined — nominally close to one of the STR arrays. Thermistor strings could be added to these locations, but they would otherwise have no surface expression.

4.3. Intensive Sampling Period

During a 7–10-day window of the full experiment, intensive focused sampling will occur that involves drifters deployments, vessel-based observations, and AUV sampling.

4.3.1. Surf Zone and Inner Shelf Drifters
(Spydell, MacMahan, Feddersen, Reniers)

Drifters deployed in the field experiment are capable of surf zone and shelf (low wind drag) observations. They are based on long-standing designs and were used in RIVET-II and CARTHE SCOPE experiments. They are also stackable and portable so they can be deployed and re-deployed using small boats in multiple locations and in large quantities, which is important for Lagrangian statistics (*LaCasce*, 2008). On many days, drifters will be released in both the SZ and inner shelf regions during a range of environmental conditions, with typical drift times of 8+ hrs and displacements of 4 km cross-shore and 20 km alongshore. UNOLS ship time will be scheduled for drifter deployments. To study the eddy field in the SZ and inner shelf, single and two-particle Lagrangian statistics will be derived from the drifter observations and analyzed using the methods of *Spydell et al.* (2007).

4.3.2. SWIFT Drifters and Surveys
(Thomson, Moulton)

Surface Wave Instrumentation Float with Tracking (SWIFT) drifters (*Thomson*, 2012; www.apl.uw.edu/swift) will be deployed to measure turbulence profiles in a wave-following reference frame in the STR. The turbulence measurements use up-looking, pulse-coherent Doppler profilers. Secondary measurements include directional wave spectra, surface winds, salinity, water temperature, air temperature, and surface images. The latest version (v3.3) includes onboard processing, Iridium SBD data telemetry, and month-long endurance. An alternate version uses a down-looking Doppler profiler (up to 20 m depth).

Approximately six SWIFTs will be released and allowed to drift throughout the domain on missions of up to one month (Figure 6). Likely, they will drift out of the domain or onto the beach before the month is up, at which point they can be reset at several established drift release points (possibly the surface wave mooring locations). Near-surface turbulence observations will be integrated with near-bottom turbulence observations (section 4.1.3). Drift speeds track the upper meter of the ocean surface, minus an approximately 5% wind slip. SWIFT is tracked in real time using a Garmin Astro radio collar (continuous updates with 10-km range), AIS beacon, and an Iridium modem (updates once per hour with global coverage).

A coastal vessel from APL-UW will be used to survey among the drifters, collecting atmospheric flux measurements (covariance wind stresses and heat fluxes) and near surface profiles of C, T, and velocity.

A fleet of eight smaller ‘microSWIFTs’ may be deployed on daily missions. These drifters measure waves and surface currents (drift) only. They have a deployment endurance of 12 hours and local tracking only.

4.3.3. Autonomous Undersea Systems
(Terrill)

A REMUS 100 and a surf zone crawler are available for focused deployments during a portion of the experiment. These systems map temperature, velocity, CTD, and optical properties. A Liquid Robotics SV3 Wave Glider equipped with wave and meteorological sensors can be made available to patrol offshore in waters of 20 m or deeper.

4.3.4. Vessel Surveys
(Lerczak, Barth, MacKinnon, Waterhouse)

Surveys will be conducted from two platforms, a UNOLS vessel in water depths of 20–100 m and a small vessel (~50 ft) in water depths of 10–30 m. The vessels will be equipped with a side-mounted ADCP, bow chain, and a towed sampling platform (either a MiniBAT or profiling CTD). The small vessel will be equipped with a side-mounted ADCP and a rapidly profiling CTD package.

After mooring operations are complete, the vessels will coordinate sampling along- and cross-shore within the mooring array to define the variability of the water column in the along- and cross-shore directions. Water column velocities will be measured from the very near surface (~1 m) to the bottom with the combined over-boarding ADCP and ship-mounted ADCP.

4.3.5. High-frequency Acoustic Imaging
(Moum)

Two high-frequency (120 kHz) echosounders will be deployed on project vessels. These will be used to image the flow field. Investigators based on the vessels will be responsible for installations.

4.4. Remote Sensing Observations

4.4.1. SAR and IR Imaging
(Farquharson, Chickadel, Moulton)

An integrated airborne instrument package, including a dual-beam, along-track interferometric synthetic aperture radar (the APL-UW ATI-SAR), thermal infrared (TIR) and optical cameras, and a point-measuring lidar, will be used to observe and characterize the surface signature and spatio-temporal development of internal waves, fronts, and rip currents. The airborne platform will be flown over the broad inner shelf region of interest, spanning approximately 6 km in the cross-shore and 15 km in the alongshore (~45-min repeat time), providing a wide field of view to observe sub-mesoscale inner shelf processes; additional tracks will be flown over the STR (Figure 6, gray rectangle).

To track internal wave packets as they propagate over the inner shelf including the STR, aircraft tracks will be oriented parallel to the internal wave crests and progressively shifted shoreward (Figure 8). Multiple wave crests could be imaged in one swath (2–3 km wide). The remotely sensed surface velocity and temperature measurements will be combined with physical constraints to infer subsurface properties; estimates of surface velocities from ATI-SAR (*Romeiser*, 2013) and particle image velocimetry (PIV) from TIR images will be compared and tested. To address the role of internal bores and rip currents in controlling stratification and exchange (*Hally-Rosendahl et al.*, 2014) in the STR, an alongshore transect encompassing the STR and spanning a long alongshore range and discreet, focused imaging locations will be repeated frequently during the intensive sampling period.

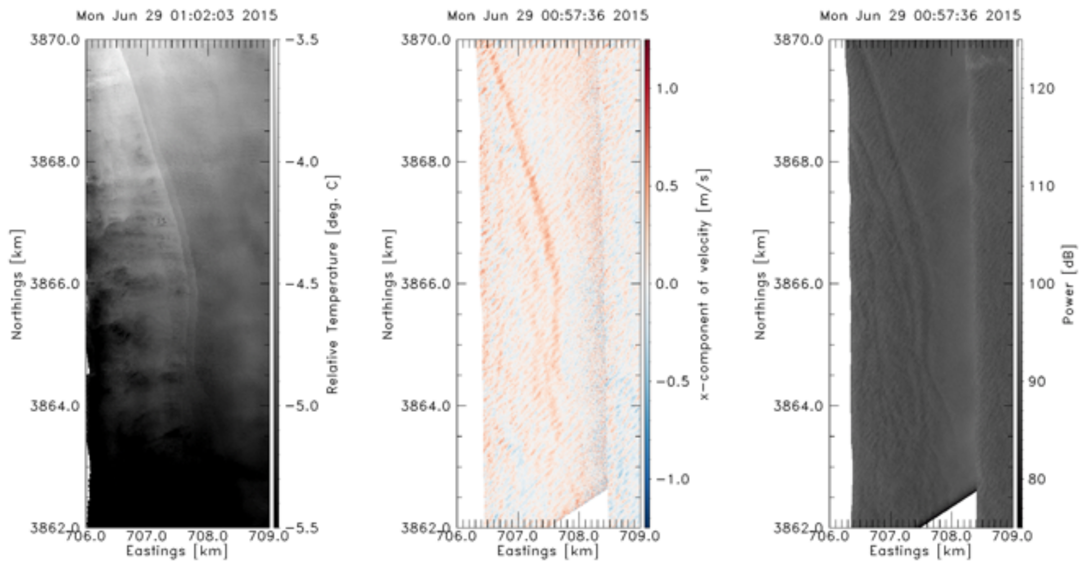

Figure 8. Surface signatures of an internal wave offshore of Point Sal, CA. (left) Surface temperature signature from aircraft-based infrared camera. The internal wave temperature difference is approximately 0.5 K. (center) East (x) component of surface velocity signature from aircraft-based along-track interferometric SAR. (right) SAR image representing surface roughness. From *Farquharson and Chickadel* (2016).

4.4.2. Airborne Remote Sensing (Melville, Lenain)

The surface expression of NLIWs are due primarily to the modulation of the fine scale scatterers on the ocean surface and the thermal signature when they break the cool-skin layer. The Modular Aerial Sensing System (MASS; *Melville et al*., 2016) includes a scanning topographic waveform lidar, IR, visible, and hyperspectral imagery, and a bathymetric waveform lidar. The MASS will be used to measure surface and internal wave processes along the boundaries of and within the Inner Shelf DRI main field experiment site. Surface wave processes will include the evolution of the directional wave spectra, the Stokes drift inferred from the wave spectra, surface currents from correlation analysis of the IR imagery, wave breaking statistics (*Sutherland and Melville*, 2013) from visible and IR imagery, surface signatures of Langmuir circulations, and mixing from the IR imagery (Figure 9).

In clearer waters, lidar will measure bathymetry out to 10 m depth, facilitating STR science. It will also provide measurements in the water column of sediment and bubble transport from headland separations as observed in the DRI 2015 pilot experiments (Figure 1, bottom right). These data will test models of surface wave growth, propagation, refraction, and dissipation. The breaking statistics and Langmuir circulation data will contribute to models of mixing in the water column. Measurements of the vertical vorticity generated by breaking in the SZ will test cross-shore transport and turbulence models.

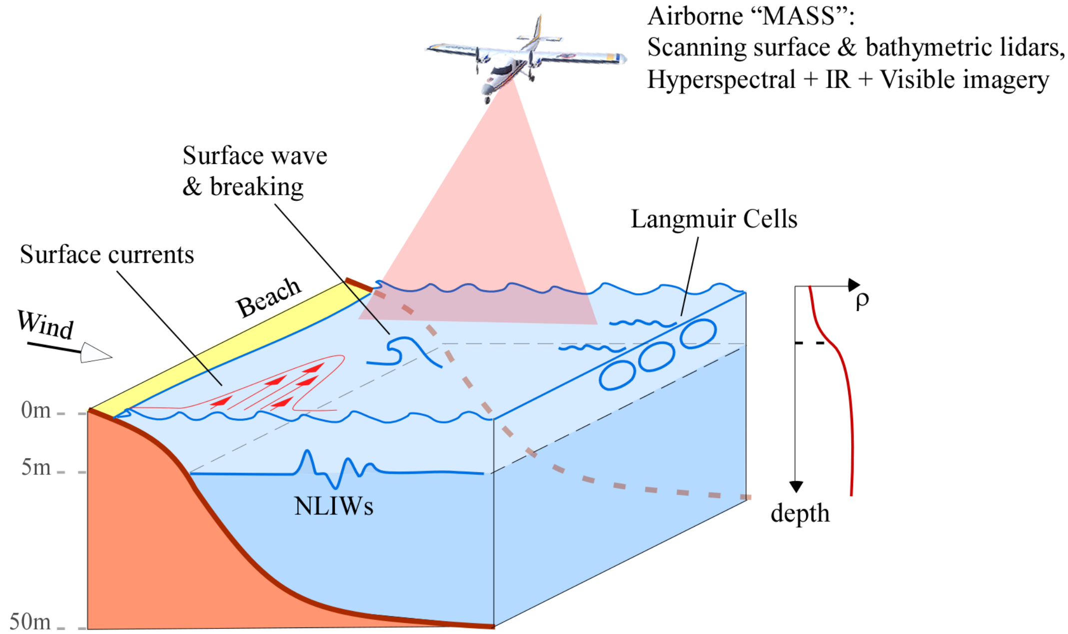

Figure 9. Schematic of the airborne remote sensing observations.

4.4.3. X-band Radar
(Haller, Terrill, Honegger)

Synoptic, marine radar observations of waves and episodic currents will be collected at two or three locations within the Inner Shelf DRI domain (Figure 6, yellow shaded regions). Specific locations and deployment durations remain to be determined owing to logistical uncertainties. Marine radar operations were conducted from Vandenberg Air Force Base during the DRI 2015 pilot experiment. The radar field of view extended to Point Sal to the north, and approximately 6 km to the south, when operating in short pulse mode. In medium pulse mode, the radar sampled out to 12 km.

An open beach radar station to the north of Point Sal will concentrate observations on the frequent rip currents (e.g., Figure 10). Typically, the system operates at 60–70% duty cycle (20-min collections every 30 min). This location will likely not have shore power and will have to be operated from a mobile trailer with a jack-up tower. From such low-altitude installations (10–15 m above sea level), wave signals are expected to be limited to ~2 km from the antenna location. This should provide good coverage of rip currents but limited coverage of internal wave propagation. A second system will allow extended range for internal wave detection. These sites will be coordinated with other ground-based radar stations to provide complementary coverage distributed along the coast to meet the broader requirements of the Inner Shelf DRI.

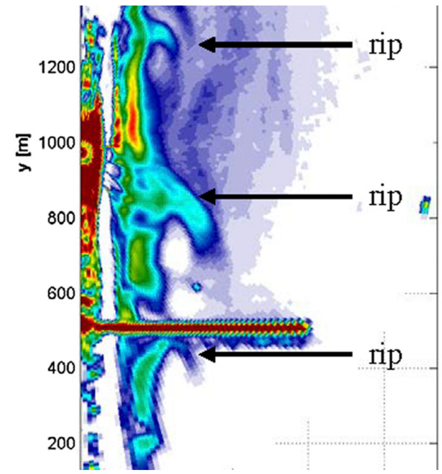

Figure 10. Radar image showing rip current outbreak event at Duck, NC. From *Haller et al*. (2014).

4.4.4. *Satellite Remote Sensing (Graber, Romeiser)*

We will utilize high-resolution SAR (~1–3-m ground resolution) and electro-optical (EO) (< 1-m ground resolution) satellite observations to make repeated measurements of the NLIWs as they propagate from offshore towards the inner shelf and coast. The measurements will also be used to derive snapshots of the surface wind vector field over the Inner Shelf DRI region to provide context between offshore forcing and the local (inner shelf) response as well as the changes in the wind stress field due to the presence of internal and surface gravity waves. TerraSAR-X aperture switching mode configuration allows for single image along-track interferometry imaging. These interferometric pairs will be used to compute the range varying surface current velocities along the coast of the Inner Shelf DRI domain (e.g., Figure 11). Furthermore, we will use SAR and EO images to provide context for surface features such as fronts and eddies as well as the presence of surfactants.

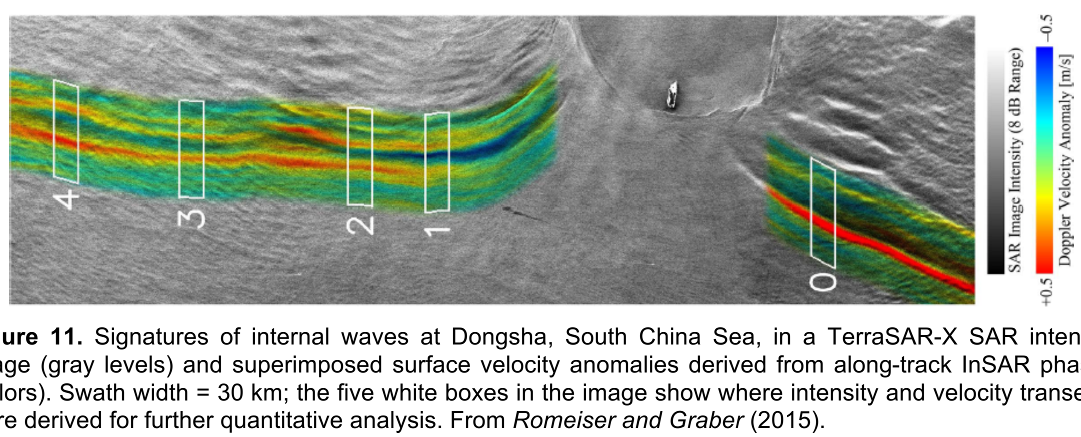

Figure 11. Signatures of internal waves at Dongsha, South China Sea, in a TerraSAR-X SAR intensity image (gray levels) and superimposed surface velocity anomalies derived from along-track InSAR phases (colors). Swath width = 30 km; the five white boxes in the image show where intensity and velocity transects were derived for further quantitative analysis. From *Romeiser and Graber* (2015).

4.4.5. *Vessel-based Remote Sensing (Graber, Romeiser)*

Complementary to the land-based observations with X-band radar, we plan to deploy a Doppler marine radar (DMR) operating at 9.4 GHz (X-band) and utilizing vertical polarization on transmit and receive (VV) on the R/V *Oceanus*. The DMR differs from the typical WaMoS marine radar in two important ways:

- It is a coherent radar, i.e., it measures a complex signal consisting of phase and amplitude; the WaMoS, in constrast, is incoherent, yielding backscatter intensity only.
- It uses a VV antenna, whereas WaMoS uses a standard HH (i.e., horizontally polarized) antenna.

In principle, the phase information from the DMR will be analyzed to yield surface current velocities. Furthermore, it offers an improved estimate of significant wave height that does not require an empirical calibration step (*Carrasco et al.*, 2016). The advantage of VV-polarized radars over HH ones is that they produce better wave and near-surface current results under low wind conditions (e.g., *Huang and Gill*, 2012).

Placing the DMR on the ship will allow for greater flexibility to track and follow NLIWs, repeatedly transecting the wave trains to measure the evolution from deep to shallow water. This was done successfully during the NLIWI 2006 experiment near Hudson Canyon in the Mid-Atlantic Bight. DMR can be used to construct surface current maps showing frontal features and small-scale eddies (e.g., Figure 12). This will also provide surface vector winds and directional wave properties along the ship track over a swath of ~4–6 km defined by rotating the antenna and assuming no interference from other ship structures.

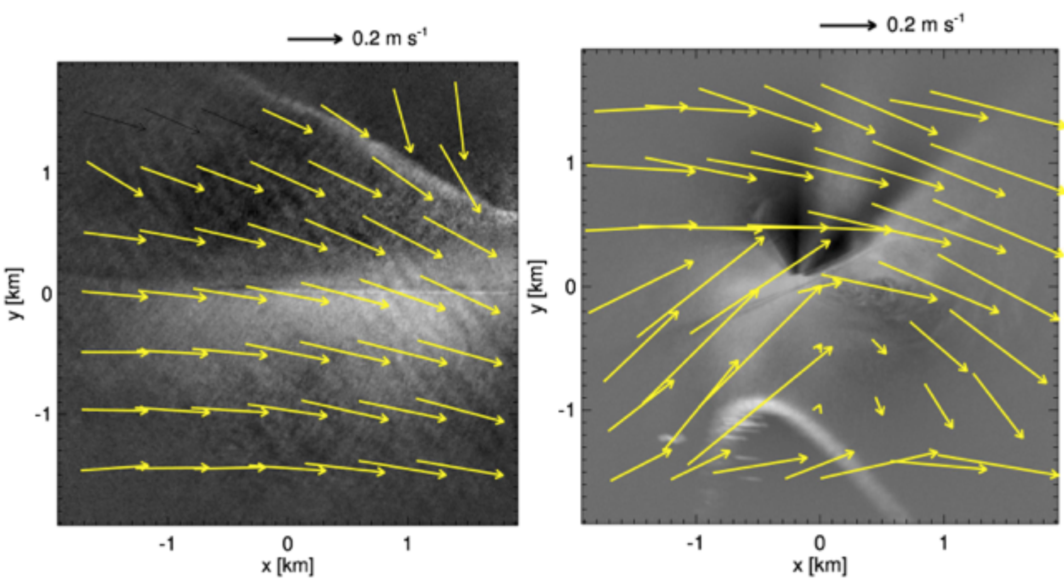

Figure 12. Examples of near-surface current maps exhibiting a front (left) and a small-scale eddy near Velasco Reef (right).

4.5. Meteorological and Radiative Observations

4.5.1. Radiometer Observations (MacMahan, Feddersen)

Radiometers will be deployed with the X-band radar systems at two locations near the shoreline north and south of Point Sal separated by 10 km. These will provide measurements of shortwave heat fluxes for observational analysis of diurnal inner shelf temperature variability and model studies. They will also provide insight into local variations in short-wave radiative heating due to local variations in cloud cover, potentially induced by the persistent ocean temperature gradient north and south of Point Sal.

4.5.2. Meterological Observations (Thomson, Terrill)

The X-band radar stations will be outfitted with wind and temperature sensors for the duration of the experiment. Additional measurements will be made from the APL-UW coastal vessel while conducting surveys during drifter releases. The shipboard measurements will include direct covariance wind stresses, long- and short-wave radiation, and temperature. The SWIFT drifters will also measure wind and air temperature.

5. Modeling

To plan, interpret, and diagnose the observational data collected in the field experiment we propose a multi-scale ocean modeling system, using the Coupled Ocean Atmosphere Wave and Sediment Transport (COAWST) model (*Warner et al*., 2010) and the Regional Ocean Modeling System (ROMS; *Haidvogel et al*., 2008) Generalized Stability Analysis (GSA; *Moore et al*., 2004) tools. These will be used to simulate and diagnose observed ocean variability in the inner shelf region, and provide a model–observations integrated platform to address the key science questions and goals of the Inner Shelf DRI (section 3; e.g., Figure 13).

5.1. COAWST Model

We have implemented the COAWST (coupled SWAN/ROMS) model in a multi-scale nested modeling framework for the inner shelf that combines observations and model output to hindcast the circulation dynamics during the period of the field campaign. COAWST includes wave shoaling, refraction, and depth-limited breaking. ROMS is a three-dimensional (3D) ocean circulation model solving the Reynolds averaged Navier–Stokes equations with the hydrostatic and Boussinesq approximations (*Shchepetkin and McWilliams*, 2005; *Haidvogel et al*., 2008; *Shchepetkin and McWilliams*, 2009). Wave–current interaction is based on the vortex force formalism (*Craik and Leibovich*, 1976), separating conservative (*McWilliams et al*., 2004) and non-conservative (breaking wave forcing) wave effects (*Uchiyama et al*., 2010; *Kumar et al*., 2012). COAWST has been validated and used in a variety of SZ, tidal inlet, inner shelf, and mid-shelf applications (*Kumar et al*., 2011, 2012; *Olabarrieta et al*., 2011; *Kumar et al*., 2015a, b).

A preliminary model configuration consists of quadruply-nested model domains with an off-line, one-way nesting technique (see *Mason et al*., 2010, *Uchiyama et al*., 2014). The model grids (Figure 14) downscale from a domain of the U.S. West Coast and Eastern Pacific (L1, resolution 1000 m), to the region from Point Conception to south of Monterey Bay (L2, resolution 600 m), to the interior Point Sal region (L3, resolution 200 m, and L4/L5, resolution 60/22 m). These domains have 42 (L1, L2, and L3) or 21 (L4) bathymetry-following vertical levels. The outermost domain L1 is forced with boundary conditions (velocity, temperature, salinity, and sea surface elevation) from nested ROMS simulations conducted for the U.S. West Coast with resolutions of 3 and 1 km. Alternatively, boundary conditions from the high-resolution HYCOM will be used. For grids L1–L4, a COAMPS simulation (resolution 3 km) provides meteorological forcing to estimate the bulk fluxes. Barotropic tidal elevation and velocities of M2, S2, N2, K2, O1, P1, and Q1, obtained from the ADCIRC tidal database, are applied on the lateral boundaries of L1. The L1 solutions are used as L2 lateral boundary conditions, every 2 hours, while L2 solutions provide L3 boundary conditions, and L3 solutions provide L4 boundary conditions, both every hour. SWAN L2 grid lateral wave boundary conditions will be derived from NOAA or Coastal Data Information Program wave boundary conditions and passed to L3 and L4.

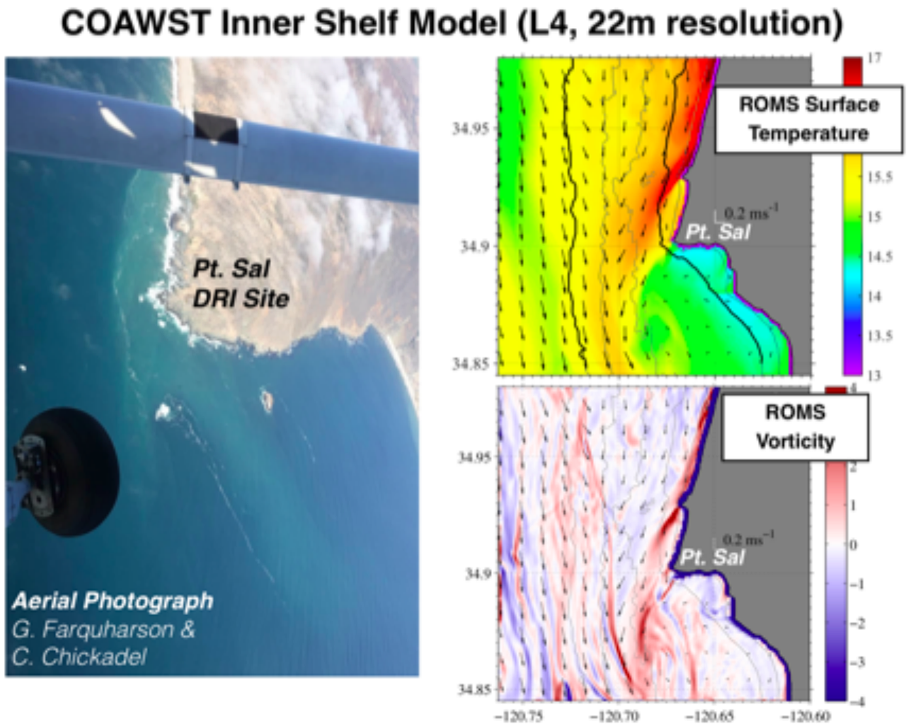

Figure 13. Comparison of an aerial photo off Point Sal along the U.S. West Coast and the output of COAWST 22-m resolution nested grid. The model sea surface temperatures and vorticity field show a clear sign of a filament developing on the lee of the cape, which is also apparent in the aerial photo.

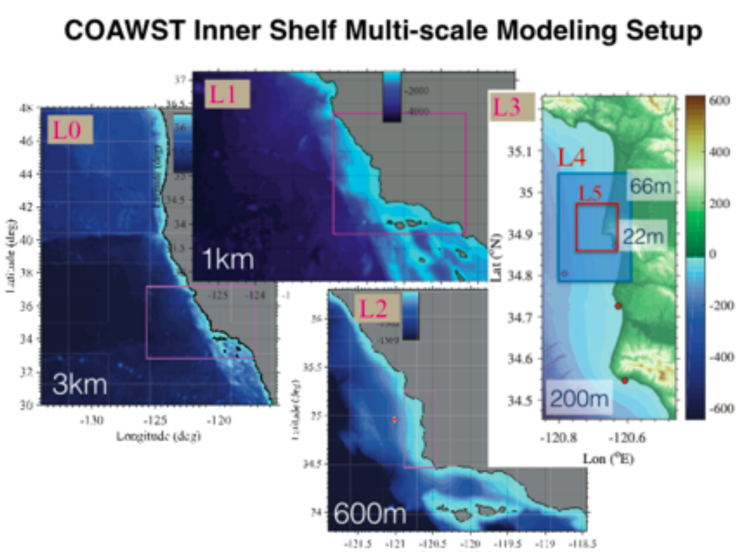

Figure 14. Grids used for simulations with four levels of successive one-way nesting. Most of the results discussed here come from L3 grid (dx = 200 m), which includes all moorings used for model–data comparison (red circles). Mid-shelf mooring is at 100 m depth (SMB). From south to north, headlands (15 m depth) with measurements are Points Arguello (ARG), Purisma (PUR), and Sal (SAL). From *Suanda et al*. (2016).

5.2. Inner Shelf Modeling Plan

Using this modeling framework we will conduct several analyses to design the field experiment and interpret the observations, leading to diagnosis of the circulation dynamics around Point Sal.

5.2.1. Hindcast of DRI 2015 Pilot Experiment Period (Miller, Edwards, Haas)

We will conduct a hindcast model simulation for the time period of the DRI 2015 pilot experiment. We will quantify the ability of the model to capture observed circulation features and perform a set of initial diagnostics on the model fields.

5.2.2. Historical Ensemble for 2000–2015 (Haas, Edwards)

The modeling of the DRI 2015 pilot experiment observations amounts to only one (inadequate) realization of the regional circulation dynamics. Thus, an ensemble of fully nested forward simulations will be performed for the same seasonal period as the DRI field work, but spanning 2000–2015. These additional runs will provide a more robust statistical sample to help understand the range of variability and how it covaries. The results will guide experiment planning, used to interpret the dynamics observed and modeled during the field campaign, and to develop and conduct the sensitivity analyses.

5.2.3. Generalized Stability Analyses (Di Lorenzo, Moore)

To further diagnose the circulation dynamics, we will also implement generalized stability analyses (GSA) tools to compute the sensitivities of inner shelf flows to surface and boundary forcings. Specifically, we will quantify the sensitivities of the flows in the inner shelf to surface and wave forcing responses (winds, heat fluxes, surface waves, etc.), boundary forcing responses (tides, coastal currents, deep ocean currents, SZ flows etc.), and intrinsic variability (instabilities, internal wave propagation, etc.) or other processes. We will use an offline approach based on linear inverse models and an online approach with the ROMS adjoint module.

5.2.4. Shelf Physical Processes (Akan, McWilliams, Romero, Shchepetkin)

A separate ROMS configuration will be used to investigate the intrinsic variability of shelf currents and stratification in the middle California region that contains the field experiment sites for both the Inner Shelf DRI and Langmuir Turbulence DRI. It will be performed with downscaling from entire California coast solutions and forced by downscaled atmospheric fields, tidal variations, and surface gravity waves. Two interaction borders will be given special attention: 1) the eddy and tidal fluxes across the upper continental slope and 2) the shelf–surf transition zone involving surf eddies erupting offshore. Several high-resolution nested subdomains in distinctive sites and synoptic conditions will expose the range of behaviors in this region (e.g., Figures 15 and 16). In addition to the DRI sites, others are planned for the sheltered Santa Barbara coastline, the northern Channel Islands with strong tidal and subtidal through-flows and

wakes, and the headlands at Point Conception exposed to wind and waves. Understanding these shelf physical regimes and processes will help inform the interpretation of the Inner Shelf DRI measurements. (Animations of sea surface temperature, surface vorticity, and surface wave height are posted on YouTube at:
https://www.youtube.com/playlist?list=PLW7ZN3pnpgo8OZEcfNboUvf-e-f8kzk V.)

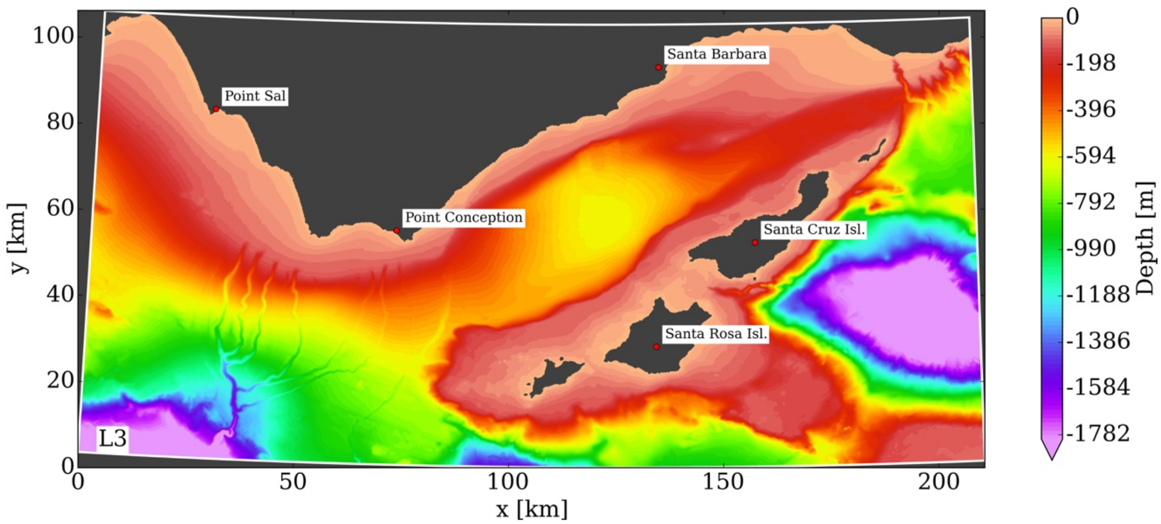

Figure 15. Bathymetry (m) in the L3 nested ROMS subdomain with a horizontal grid resolution of *dx* = 100 m. Its initial and boundary conditions are taken from large-scale circulation and atmospheric model solutions. It will be the primary testbed for shelf processes at several sites, and a further fine-scale nest will be made in a few locations to examine the shelf current interactions with the surf zone.

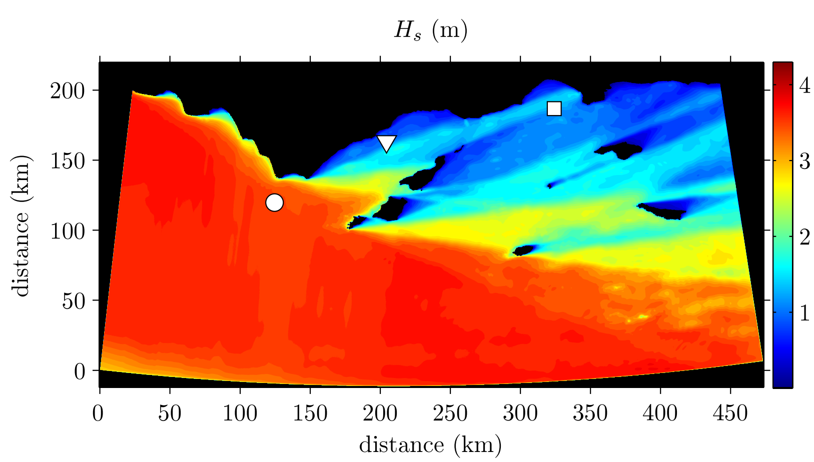

Figure 16. Simulated significant wave height H_s (m) on 24 November 2004 at 06:00 pm (UTC) using the WaveWatch III® spectral wave model. The white circle, triangle, and square indicate the location of the Harvest, Goleta, and Santa Monica Bay buoys, respectively. The domain is the next level coarser L2 subdomain (*dx* = 300 m) within which the L3 subdomain in Figure 15 is nested. It is coupled to the ROMS circulation model to investigate wave–current interaction both on the shelf and in the surf zone.

6. References

Aiki, H., and R. Greatbatch 2012: Thickness-Weighted Mean theory for the effect of surface gravity waves on mean flows in the upper ocean. *J. Phys. Oceanogr.,* **42**, 725-747.

Aiki, H., and R. Greatbatch 2013: The vertical structure of the surface wave radiation stress for circulation over a sloping bottom as given by Thickness-Weighted-Mean theory. *J. Phys. Oceanogr*., **43**, 149-164.

Alford, M.H., J.B. Mickett, S. Zhang, P. MacCready, Z. Zhao, and J. Newton, 2012: Internal waves on the Washington continental shelf. *Oceanography*, **25**, 66-79.

Apotsos, A., B. Raubenheimer, S. Elgar, and R.T. Guza, 2008: Wave-driven setup and alongshore flows observed onshore of a submarine canyon. *J. Geophys. Res*. **113**, doi:10.1029/2007JC004514.

Ardhuin, A., N. Rascle, and K.A. Belibassakis, 2008: Explicit wave-averaged primitive equations using a generalized Lagrangian mean. *Ocean Model*., **20**, 35-60.

Austin, J.A., and S.J. Lentz, 2002: The inner shelf response to wind-driven upwelling and downwelling. *J. Phys. Oceanogr*., **32**, 2171–2193.

Austin, J.A., and J.A. Barth, 2002: Variation in the position of the upwelling front on the Oregon shelf. *J. Geophys. Res*., **107**, doi:10.1029/2001JC000858.

Brown, J.A., J.H. MacMahan, A.J.H.M. Reniers, and E.B. Thornton, 2015: Field observations of surf zone–inner shelf exchange on a rip-channeled beach. *J. Phys. Oceanogr*., **45**, 2339–2355.

Bühler, O., and M. Holmes-Cerfon, 2009: Particle dispersion by random waves in rotating shallow water. *J. Fluid Mech.* **638**, 5-26.

Butman, B., P.S. Alexander, A. Scotti, R.C. Beardsley, and S.P. Anderson, 2006: Large internal waves in Massachusetts Bay transport sediments offshore. *Cont. Shelf Res*., **26**, 2029-2049.

Carrasco, R., M. Streßer, and J. Horstmann, 2016: A simple method for retrieving significant wave height from Dopplerized X-band radar. *Ocean Sci. Discuss*., doi:10.5194/os-2016-29.

Chang, M.-H., R.-C. Lien, Y.J. Yang, T.Y. Tang, and J. Wang, 2008: A composite view of surface signatures and interior properties of nonlinear internal waves: Observations and applications. *J. Atmos. Ocean. Technol*., **25**, 1218–1227.

Clark, D.B., F. Feddersen, and R.T. Guza, 2010: Cross-shore surfzone tracer dispersion in an alongshore current. *J. Geophys. Res*., **115**, doi: 10.1029/2009JC005683.

Craik, A., and S. Leibovich, 1976: A rational model for Langmuir circulations. *J. Fluid Mech*., **73**, 401–426.

Durski, S.M., and J.S. Allen, 2005: Finite-amplitude evolution of instabilities associated with the coastal upwelling front. *J. Phys. Oceanogr*., **35**, 1606–1628.

Elgar, S., R.T. Guza, B. Raubenheimer, T.H.C. Herbers, and E. Gallagher, 1997: Spectral evolution of shoaling and breaking waves on a barred beach. *J. Geophys. Res*., **102**, 15797-15805.

Farquharson, G., and C.C. Chickadel, 2016: Airborne remote sensing of inner shelf submesoscale processes. In *Proc., Ocean Sciences 2016*, 21-26 February, New Orleans, #EC24B-1083 (AGU, ASLO, and The Oceanography Society, 2016).

Feddersen, F., R.T. Guza, S. Elgar, and T.H.C. Herbers, 1998: Alongshore momentum balances in the nearshore. *J. Geophys. Res*., **103**, 15667-15676.

Feddersen, F., 2014: The generation of surfzone eddies in a strong alongshore current, *J. Phys. Oceanogr*., **44**, doi: 10.1175/JPO-D-13-051.1.

Feddersen, F., J.H. Trowbridge, and A.J. Williams, 2007: Vertical structure of dissipation in the nearshore. *J. Phys. Oceanogr*., **37**, 1764-1777.

Fewings M.R., S.J. Lentz, and J. Fredericks, 2008: Observations of cross-shelf flow driven by cross-shelf winds on the inner continental shelf. *J. Phys. Oceanogr.* **38**, 2358–2378.

Fujimura, A., A. Reniers, C. Paris, A. Shanks, J. MacMahan, and S. Morgan, 2013: Slope-dependent biophysical modeling of surf zone larval transport. *Coast. Dynam*., 661-670.

Haidvogel, D.B., et al., 2008: Ocean forecasting in terrain-following coordinates: Formulation and skill assessment of the regional ocean modeling system. *J. Comput. Phys*., **227**, 3595–3624.

Haller, M. C., D. Honegger, and P.A. Catalán, 2014: Rip current observations via marine radar. *J. Waterway*, **140**, 115-124, doi:10.1061/(ASCE)WW.1943-5460.0000229.

Hally-Rosendahl, K., F. Feddersen, and R.T. Guza, 2014: Cross-shore tracer exchange between the surfzone and inner-shelf. *J. Geophys. Res*., **119**, 4367-4388.

Hansen, J.E., T.T. Janssen, B. Raubenheimer, F. Shi, P.L. Barnard, and I.S. Jones, 2014: Observations of surf zone alongshore pressure gradients onshore of an ebb-tidal delta. C*oast. Eng.*, **91**, 251-260.

Hasselmann, K. 1970: Wave-driven inertial oscillations. *Geophys. Fluid Dyn*., **1**, 463-502.

Helfrich, K.R., 1992: Internal solitary wave breaking and run-up on a uniform slope, *J. Fluid Mech*., **243**, 133-154.

Herbers, T.H.C., and T.T. Janssen, 2016: Lagrangian surface wave motion and infragravity Stokes drift fluctuations. *J. Phys. Oceanogr.*, **46**, 1009-1021.

Herbers, T.H.C., S. Elgar, and R.T. Guza, 1995: Generation and propagation of infragravity waves., *J. Geophys. Res*., **100,** 24,863-24,872.

Herbers, T.H.C., S. Elgar, and R.T. Guza, 1999: Directional spreading of waves in the nearshore. *J. Geophys. Res*., **104**, 7683-7693.

Herterich, K., and K. Hasselmann, 1982: The horizontal diffusion of tracers by surface waves. *J. Phys. Oceanogr.,* **12**, 704-711.

Hogg, N.G., 1971: Longshore current generation by obliquely incident internal waves. *Geophys. Fluid Dyn*., **2**, 361-376.

Huang, W., and E. Gill, 2012: Surface current measurement under low sea state using dual polarized X-band nautical radar. *IEEE J. Sel. Topics Appl. Earth Observ. In Remote Sens*., **5**, 1868-1873.

Jackson, C.R., and J.R. Apel, 2004: *Synthetic Aperture Radar Marine User's Manual*. NOAA/NESDIS, Silver Spring, MD, USA, 427 pp.

Janssen, T.T., T.H.C. Herbers, and J.A. Battjes, 2008: Evolution of ocean wave statistics in shallow water: Refraction and diffraction over seafloor topography. *J Geophys. Res.*, **113**, C03024.

Janssen, T.T., J.A. Battjes, and A.R. Van Dongeren, 2003: Long waves induced by short-wave groups over a sloping bottom. *J. Geophys. Res*., **108**, doi: 10.1029/2002JC001515.

Johnson, D., and C. Pattiaratchi, 2006: Boussinesq modelling of transient rip currents. *Coast. Eng*., **53**, 419439.

Kirincich, A., 2016: The occurrent, drivers, and implications of submesoscale eddies on the Martha's Vineyard inner shelf. *J. Phys. Oceanogr*., **46**, 2645-2662.

Kohut, J.T., S.M. Glenn, and R.J. Chant, 2004: Seasonal current variability on the New Jersey inner shelf. *J. Geophys. Res*., **109**, doi:10.1029/2003JC001963.

Kumar, N., and F. Feddersen, 2016: The effect of Stokes drift and transient rip currents on the inner-shelf, part 1: No stratification. *J. Phys. Oceanogr*., in review.

Kumar, N., F. Feddersen, S. Suanda, Y. Uchiyama, and J. McWilliams, 2015a: Mid- to inner-shelf coupled ROMS-SWAN model-data comparison of currents and temperature: Diurnal and semi-diurnal variability. *J. Phys. Oceanogr*., **46**, 841-862, doi:10.1175/JPO-D-15-0103.1.

Kumar, N., F. Feddersen, Y. Uchiyama, J. McWilliams, and W. O'Reilly, 2015b: Midshelf to surfzone coupled ROMS-SWAN model data comparison of waves, currents, and temperature: Diagnosis of subtidal forcings and response. *J. Phys. Oceanogr*., **45**, 1464-1490, doi:10.1175/JPO-D-14-0151.1.

Kumar, N., G. Voulgaris, and J.C. Warner, 2011: Implementation and modification of a three-dimensional radiation stress formulation for surf zone and rip-current applications. *Coast. Eng*., **58**, 1097–1117.

Kumar, N., G. Voulgaris, J.C. Warner, and M. Olabarrieta, 2012: Implementation of the vortex force formalism in the coupled ocean-atmosphere-wave-sediment transport (COAWST) modeling system for inner shelf and surf zone applications. *Ocean Model*., **47**, 65–95.

LaCasce, J.H., 2008: Statistics from Lagrangian observations. *Prog. Oceanogr*., **77**, 1–29.

Leichter, J.J., G. Shellenbarger, S.J. Genovese, and S.R. Wing, 1998: Breaking internal waves on a Florida (USA) coral reef: A plankton pump at work? *Mar. Ecol. Prog. Ser*., **166**, 83-97.

Lentz S.J., M.R. Fewings, P. Howd, J. Fredericks, and K. Hathaway, 2008: Observations and a model of undertow over the inner continental shelf. *J. Phys. Oceanogr.* **38**, 2341–2357.

Lentz, S.J. and M.R. Fewings, 2012: The wind- and wave-driven inner shelf circulation. *Ann. Rev. Mar. Sci*, **4**, 317-343.

Lentz, S.J., R.T. Guza, S. Elgar, F. Feddersen, and T.H.C. Herbers, 1999: Momentum balances on the North Carolina inner shelf. *J. Geophys. Res*., **104**, 18,205–18,226.

Lerczak, J., C. Winant, and M. Henderschott, 2003: Observations of the semidiurnal internal tide on the Southern California slope and shelf. *J. Geophys. Res*., **108**, doi:10.1029/2001JC001128.

Long, J.W., and H. Özkan-Haller, 2005: Offshore controls on nearshore rip currents. *J. Geophys. Res*., **110**, doi:10.1029/2005JC003018.

Long, J.W., and H.T. Özkan-Haller, 2009: Low-frequency characteristics of wave group-forced vortices. *J. Geophys. Res*., **114**, doi:10.1029/2008JC004894.

Lucas, A.J., P.J.S. Franks, and C.L. Dupont, 2011: Horizontal internal-tide fluxes support elevated phytoplankton productivity over the inner continental shelf. *Limnol. Oceanogr*., **1**, 56–74.

Lund, B., H. . Graber, and R. Romeiser, 2012: Wind retrieval from shipborne nautical X-band radar data. *IEEE Trans. Geosci. Remote Sens*., **50**, 3800-3811.

MacKinnon, J.A., and M.C. Gregg, 2003: Shear and baroclinic energy flux on the summer New England shelf. *J. Phys. Oceanogr*., **33**, 1462-1475.

MacMahan, J.H., A.J.H.M. Reniers, and E.B. Thornton, 2010: Vortical surf zone fluctuation with O(10) min period. *J. Geophys. Res*., **115**, doi:10.1029/2009JC005383.

Marmorino, G.O., et al., 2004: Onshore propagation of a buoyant ocean front observed using a shore-based marine radar. *Cont. Shelf Res*., **24**(9), 951–964.

Marmorino, G.O., G.B. Smith, and W.D. Miller, 2013: Infrared remote sensing of surf-zone eddies. *IEEE J. Selec. Top. App. Earth Obs. Remote Sens*., **6**, 1710-1718.

Mason, E., J. Molemaker, A.F. Shchepetkin, F. Colas, J.C. McWilliams, and P. Sangrà, 2010: Procedures for offline grid nesting in regional ocean models. *Ocean Model*., **35**, 1–15.

McWilliams, J.C., and J.M. Restrepo, 1999: The wave-driven ocean circulation, *J. Phys. Oceanogr*., **29**, 2523-2540.

McWilliams, J.C., J.M. Restrepo, and E.M. Lane, 2004: An asymptotic theory for the interaction of waves and currents in coastal waters. *J. Fluid Mech.*, **511**, 135-178.

Mellor, G. 2003: The three-dimensional current and surface wave equations. *J. Phys. Oceanogr.*, **33**, 1978-1989.

Melville, W.K., and K.R. Helfrich, 1987: Transcritical two-layer flow over topography. *J. Fluid Mech*., **178**, 31–52.

Melville, W.K., L. Lenain, D. Cayan, M. Kahru, J. Kleissl, P. Linden, and N. Statom, 2016: The Modular Aerial Sensing System. *J. Atmos. Ocean. Technol.*, **33**, 1169-1184.

Moore, A.M., H.G. Arango, E. Di Lorenzo, B.D. Cornuelle, A.J. Miller, and D.J. Neilson, 2004: A comprehensive ocean prediction and analysis system based on the tangent linear and adjoint of a regional ocean model. *Ocean Model*., **7**, 227-258, doi:10.1016/j.ocemod.2003.11.001.

Moum, J.N., and J.D. Nash, 2009: Mixing measurements on an equatorial ocean mooring. *J. Atmos. Ocean. Technol*., **26**, 317-336.

Moum, J.N., 2015: Ocean speed and turbulence measurements using pitot-static tubes on moorings. *J. Atmos. Ocean. Technol*., **32**, 1400-1413.

Moum, J.N., D.M. Farmer, W.D. Smyth, L. Armi, and S. Vagle, 2003: Structure and generation of turbulence at interfaces strained by internal solitary waves propagating shoreward over the continental shelf. *J. Phys. Oceanogr*., **33**, 2093-2112.

Nash, J.D., S.M. Kelly, E.L. Shroyer, J.N. Moum, and T.F. Duda, 2012: The unpredictable nature of internal tides on continental shelves. *J. Phys. Oceanogr.*, **42**, 1981–2000, doi: 10.1175/JPO-D-12-028.1.

Olabarrieta, M., J.C. Warner, and N. Kumar, 2011: Wave-current interaction in Willapa Bay, *J. Geophys. Res.*, **116**, doi: 10.1029/2011JC007387.

Polton, J.A., D.M. Lewis, and S.E. Belcher, 2005: The role of wave-induced Coriolis-Stokes forcing on the wind-driven mixed layer. *J. Phys. Oceanogr.,* **35**, 444-457.

Ramos, R.J., B. Lund, and H.C. Graber, 2009: Determination of internal wave properties from X-band radar observations. *Ocean Eng.*, **36**, 1039-1047.

Reniers, A.J.H.M., J.A. Roelvink, and E.B. Thornton, 2004: Morpho-dynamic modeling of an embayed beach under wave group forcing. *J. Geophys. Res.*, **109**, doi:10.1029/2002JC001586.

Reniers, A.J., J.H. MacMahan, F.J. Beron-Vera, and M.J. Olascoaga, 2010: Rip-current pulses tied to Lagrangian coherent structures. *Geophys. Res. Lett.*, **37**, doi: 10.1029/2009GL041443.

Reniers, A.J.H.M., J.H. MacMahan, E.B. Thornton, T.P. Stanton, M. Henriquez, J.W. Brown, J.A. Brown, and E. Gallagher, 2009: Surf zone surface retention on a rip-channeled beach. *J. Geophys. Res.*, **114**, doi: 10.1029/2008JC005153.

Romeiser, R., 2013: The future of SAR-based oceanography: High-resolution current measurements by along-track interferometry. *Oceanography*, **26**, doi:10.5670/oceanog.2013.37.

Romeiser, R., and H.C. Graber, 2015: Advanced remote sensing of internal waves by spaceborne along-track InSAR-A demonstration with TerraSAR-X. *IEEE Trans. Geosci. Remote Sens.*, **53**, 6735-6751.

Sanderson, B.G., and A. Okubo, 1988: Diffusion by internal waves. *J. Geophys. Res.*, **93**, 3570-3582.

Scotti, A., and J. Pineda, 2004: Observations of very large and steep internal waves of elevation near the Massachusetts coast. *Geophys. Res. Lett.*, **31**, doi:10.1029/2004GL021052.

Scotti, A., R.C. Beardsley, B. Butman, and J. Pineda, 2008: Shoaling of nonlinear internal waves in Massachusetts Bay. *J. Geophys. Res.*, **113**, doi: 10.1029/2008JC004726.

Shchepetkin, A. F., and J.C. McWilliams, 2005: The Regional Oceanic Modeling System (ROMS): A split-explicit, free-surface, topography-following-coordinate oceanic model. *Ocean Model.*, **9**, 347–404.

Shchepetkin, A.F., and J.C. McWilliams, 2009: Correction and commentary for "Ocean forecasting in terrain-following coordinates: Formulation and skill assessment of the regional ocean modeling system" by Haidvogel et al., *J. Comp. Phys.*, **227**, 3595–3624. *J. Comp. Phys.*, **228**, 8985–9000.

Shroyer, E.L., J.N. Moum, and J.D. Nash, 2011: Nonlinear internal waves over New Jersey's continental shelf. *J. Geophys. Res.*, **116**, doi:10.1029/2010JC006332.

Sinnett, G., and F. Feddersen, 2014: The surf zone heat budget: The effect of wave heating, *Geophys. Res. Lett.*, **41**, 7217-7226.

Smit, P.B., and T.T. Janssen, 2013: The evolution of inhomogeneous wave statistics through a variable medium. *J. Phys. Oceanogr.*, **43**, 1741–1758.

Smit, P.B., T.T. Janssen, and T.H.C. Herbers, 2015: Stochastic modeling of coherent wave fields over variable depth. *J. Phys. Oceanogr.*, **45**, 1139–1154.

Smith, J., 2006: Observed variability of ocean wave Stokes drift, and the Eulerian response to passing groups. *J. Phys. Oceanogr.,* **36**, 1381-1402.

Spydell, M., and F. Feddersen, 2009: Lagrangian drifter dispersion in the surf zone: Directionally spread, normally incident waves. *J. Phys. Oceanogr*., **39**, 809–830.

Spydell, M., F. Feddersen, R.T. Guza, and W.E. Schmidt, 2007: Observing surf-zone dispersion with drifters. *J. Phys. Oceanogr*., **37**, 2920–2939.

Srokosz, M.A. and M.S. Longuet-Higgins, 1986: On the skewness of sea-surface elevation. *J. Fluid Mech.*, **164**, 487-497.

Suanda, S.H., and F. Feddersen, 2015: A self-similar scaling for cross-shelf exchange driven by transient rip currents. *Geophys. Res. Lett*., **42**, 5427-5434.

Suanda, S.H., J.A. Barth, R.A. Holman, and J. Stanley, 2014: Shore-based video observations of nonlinear internal waves across the inner shelf. *J. Atmos. Ocean. Technol*., **31**, 714-728.

Suanda, S.H., S. Perez, and F. Feddersen, 2016: Evaluation of a source-function wavemaker for generating random directionally spread waves in the sea-swell band. *Coast. Eng*., **114**, doi:10.1016/j.coastaleng.2016.04.006.

Sutherland, P., and W.K. Melville, 2013: Field measurements and scaling of ocean surface wave-breaking statistics. *Geophys. Res. Lett.*, **40**, 3074-3079.

Thomson, J., 2012: Wave breaking dissipation observed with SWIFT drifters. *J. Atmos. Ocean. Technol*., **29**, 1866–1882.

Trowbridge, J., and S. Elgar, 2001: Turbulence measurements in the surf zone. *J. Phys. Oceanogr*., **31**, 2403-2417.

Uchiyama, Y., E.Y. Idica, J.C. McWilliams, and K.D. Stolzenbach, 2014: Wastewater effluent dispersal in Southern California bays. *Cont. Shelf Res*., **76**, 36-52

Uchiyama, Y., J.C. McWilliams, and A.F. Shchepetkin, 2010: Wave-current interaction in an oceanic circulation model with a vortex-force formalism: Application to the surf zone. *Ocean Model*., **34**, 16–35.

Walter, R.K., C.B. Woodson, R.S. Arthur, O.B. Fringer, and S.G. Monismith, 2012: Nearshore internal bores and turbulent mixing in southern Monterey Bay. *J. Geophys. Res*., **177**, doi:10.1029/2012JC008115.

Walter, R.K., M.E. Squib, C.B. Woodson, J.R. Koseff, and S.G. Monismith, 2014a: Stratified turbulence in the nearshore coastal ocean: Dynamics and evolution in the presence of internal bores. *J. Geophys. Res*., **119**, doi:10.1002/2014JC010396.

Walter, R.K., C.B. Woodson, P.L. Leary, and S.G. Monismith, 2014b: Connecting wind-driven upwelling and offshore stratification to nearshore internal bores and oxygen variability. *J. Geophys. Res*., **119**, doi:10.1002/2014JC009998.

Warner, J.C., B. Armstrong, R. He, and J. B. Zambon, 2010: Development of a coupled ocean–atmosphere–wave–sediment transport (COAWST) modeling system. *Ocean Model*., **35**, 230–244.

Winant, C.D., 1974: Internal surges in coastal waters. *J. Geophys. Res*., **79**, 4523-4526.

Woodson, C.B., 2013: Spatiotemporal variation in cross-shelf exchange across the inner shelf of Monterey Bay, California. *J. Phys. Oceanogr*., **43**, 1648-1665.

Woodson, C.B., et al., 2011: Observations of internal wave packets propagating along-shelf in northern Monterey Bay, *Geophys. Res. Lett*., **38**, doi: 10.1029/2010GL045453.

Xu, Z., and A.J. Bowen, 1994: Wave- and wind-driven flow in water of finite depth. *J. Phys. Oceanogr.,* **24,** 1850–1866.

Zhang, S., M.H. Alford, and J.B. Mickett, 2015: Characteristics, generation and mass transport of nonlinear internal waves on the Washington continental shelf. *J. Geophys. Res*., **120**, 741-758.

REPORT DOCUMENTATION PAGE

Form Approved
OMB No. 0704-0188

1. REPORT DATE *(DD-MM-YYYY)*	2. REPORT TYPE	3. DATES COVERED *(From - To)*
31-10-2016	Technical Report	

4. TITLE AND SUBTITLE

Inner Shelf Dynamics Science and Experiment Plan

5a. CONTRACT NUMBER

5b. GRANT NUMBER

Calantoni, N0001416WX00044; Colosi, N0001415WX00691; Di Lorenzo, N000141410556; Farquharson and Chickadel,

5c. PROGRAM ELEMENT NUMBER

6. AUTHOR(S)

Falk Feddersen, Jack Barth, Joe Calantoni, Chris Chickadel, John Colosi, Emanuele Di Lorenzo, Chris Edwards, Gordon Farquharson, Thomas Freismuth, Hans Graber, Kevin Haas, Mick Haller, Thomas H.C. Herbers, David Honegger, Tim Janssen, Nirnimesh Kumar, Luc Lenain, James Lerczak, Jennifer MacKinnon, Jamie MacMahan, James McWilliams, Ken Melville, Arthur Miller, Andrew Moore, Melissa Moulton, James Moum, Ad Reniers, Roland Romeiser, Julian Simeonov, Matthew Spydell, Eric Terrill,

5d. PROJECT NUMBER

5e. TASK NUMBER

5f. WORK UNIT NUMBER

7. PERFORMING ORGANIZATION NAME(S) AND ADDRESS(ES)

Applied Physics Laboratory – University of Washington
1013 NE 40th Street
Seattle WA 98105

8. PERFORMING ORGANIZATION REPORT NUMBER

APL-UW TR 1602

9. SPONSORING/MONITORING AGENCY NAME(S) AND ADDRESS(ES)

Dr. Reginald Beach
Office of Naval Research
Littoral Geosciences and Optics Program
875 N. Randolph Street, Suite 1425
Arlington, VA 22203

10. SPONSOR/MONITOR'S ACRONYM(S)

11. SPONSOR/MONITOR'S REPORT NUMBER(S)

12. DISTRIBUTION/AVAILABILITY STATEMENT

Approved for public release; distribution is unlimited

13. SUPPLEMENTARY NOTES

14. ABSTRACT

The deep ocean, continental shelf, and surf zone are defined by their unique physical processes and dynamics. The nearshore region from about 50 m water depth to the outer edge of the surf zone (SZ) is known as the inner shelf. This region is characterized by overlapping and interacting surface and bottom boundary layers. At the offshore side of the inner shelf, instabilities from wind-driven currents and fronts create cross-shelf meanders and eddies. In addition, energetic nonlinear internal waves (NLIWs) are ubiquitous on the inner shelf.

To understand and predict the exchange of water properties (heat, gases, sediment, pollutants, biota) across the inner shelf over a range of temporal and spatial scales, the Office of Naval Research Inner Shelf Dynamics Departmental Research Initiative (Inner Shelf DRI) is coordinating field observations (in situ and remote sensing) coupled to numerical modeling efforts on a 50-km section

15. SUBJECT TERMS

physical oceanography, observational oceanography, air-sea interaction, remote sensing, inner shelf, surf zone, nonlinear internal waves, COAWST ocean model, littoral oceanography, coastal oceanography

16. SECURITY CLASSIFICATION OF: a. REPORT	b. ABSTRACT	c. THIS PAGE	17. LIMITATION OF ABSTRACT	18. NUMBER OF PAGES	19a. NAME OF RESPONSIBLE PERSON
unclass	unclass	unclass	unlimited	35	Jim Thomson

19b. TELEPHONE NUMBER *(Include area code)*

206-616-0858